SARS-CoV-2 invades cognitive centers of the brain and induces Alzheimer's-like neuropathology

Wei-Bin Shen[1#], James Logue[2#], Penghua Yang[1#], Lauren Baracco[2], Montasir Elahi[1], E. Albert Reece[1, 3], Bingbing Wang[1], Ling Li[4], Thomas G Blanchard[4], Zhe Han[5], Matthew B Frieman[2], Robert A Rissman[6, 7], Peixin Yang[1, 3 *]

[1]Department of Obstetrics, Gynecology & Reproductive Sciences, University of Maryland School of Medicine, Baltimore, Maryland, USA.
[2] Department of Microbiology and Immunology, University of Maryland School of Medicine, Baltimore, MD 21201, USA.
[3]Department of Biochemistry & Molecular Biology, University of Maryland School of Medicine, Baltimore, Maryland, USA.
[4]Department of Pediatrics, University of Maryland School of Medicine, Baltimore, MD, USA.
[5]Department of Medicine, University of Maryland School of Medicine, Baltimore, MD, USA.
[6]Department of Neurosciences, University of California San Diego, La Jolla, CA, 92093.
[7]Shiley-Marcos Alzheimer's Disease Research Center, University of California San Diego, La Jolla, California, 92093.
[#] These authors contribute equally to this work.
*Correspondence: Peixin Yang, PhD, Department of Obstetrics, Gynecology & Reproductive Sciences, University of Maryland School of Medicine, BRB11-039, 655 W. Baltimore Street, Baltimore, MD, 21201. Email: pyang@som.umaryland.edu, Tel: 410-706-8402, Fax: 410-706-5747.

Conflict of interest statement: The authors have declared that no conflict of interest exists

Subheading: Neurodegenerative phenotypes in COVID-19

Keywords: SARS-CoV-2; neurons; iPSC; Alzheimer's; COVID-19 brains; Alzheimer's infectious etiology; beta-amyloid; neuroinflammation; tauopathy.

Abstract

Major cell entry factors of SARS-CoV-2 are present in neurons; however, the neurotropism of SARS-CoV-2 and the phenotypes of infected neurons are still unclear. Acute neurological disorders occur in many patients, and one-third of COVID-19 survivors suffer from "brain diseases". Here, we show that SARS-CoV-2 invades the brains of five patients with COVID-19 and Alzheimer's, autism, frontotemporal dementia or no underlying condition by infecting neurons and other cells in the cortex. SARS-CoV-2 induces or enhances Alzheimer's-like neuropathology with manifestations of β-amyloid aggregation and plaque formation, tauopathy, neuroinflammation and cell death. SARS-CoV-2 infects mature but not immature neurons derived from inducible pluripotent stem cells from healthy and Alzheimer's individuals through its receptor ACE2 and facilitator neuropilin-1. SARS-CoV-2 triggers Alzheimer's-like gene programs in healthy neurons and exacerbates Alzheimer's neuropathology. A gene signature defined as an Alzheimer's infectious etiology is identified through SARS-CoV-2 infection, and silencing the top three downregulated genes in human primary neurons recapitulates the neurodegenerative phenotypes of SARS-CoV-2. Thus, SARS-CoV-2 invades the brain and activates an Alzheimer's-like program.

Introduction

The COVID-19 pandemic caused by severe acute respiratory syndrome coronavirus 2 (SARS-CoV-2) has infected at least 213 million people worldwide and 37.8 million Americans to date. SARS-CoV-2 not only causes respiratory syndromes but also leads to neurological abnormalities, with an 85% occurrence rate in patients with Alzheimer's disease [1, 2]. In fact, neurological symptoms, including hypogeusia, headache and anosmia, precede the onset of respiratory symptoms in the majority of patients with COVID-19. The major chronic sequelae of COVID-19 are expected to be cognitive decline and dementia [3]. A recent study has shown that one-third of COVID-19 survivors exhibit substantial neurological and psychiatric morbidity in the 6 months after SARS-CoV-2 infection [4]. Furthermore, the "brain disease" risk is not limited to patients who have severe COVID-19 [4]. Thus, the COVID-19 pandemic provides a unique but unwelcomed opportunity to study the contribution of SARS-CoV-2 to neurological disorders, including Alzheimer's disease.

It has been proposed that β-coronaviruses, including SARS-CoV-2, can invade the central nervous system [5]. The two coronaviruses closely related to SARS-CoV-2, Middle Eastern respiratory syndrome coronavirus (MERS-CoV) and severe acute respiratory syndrome coronavirus 1 (SARS-CoV-1), can infect the central nervous system [6, 7]. A recent study shows the presence of SARS-CoV-2 in a patient's olfactory mucosa and its neuronal projections [8]. SARS-CoV-2 RNA is present in 36.4% of brain biopsies of fatal COVID-19 cases [9]. A recent study observes the presence of SARS-CoV-2 spike protein in some brain regions in all three COVID-19 cases studied [10]. In transgenic hACE2 mice, SARS-CoV-2 is massively present in the brain at post infection day 5 [11]. In addition to olfactory transmucosal entry of SARS-CoV-2 into the central nervous system (CNS) [8], other potential routes of SARS-CoV-2 brain entry, including blood–brain barrier (BBB) passage, especially under conditions of a compromised BBB, such as in cases of Alzheimer's disease and autism [12, 13], and the infiltration of infected immune cells

have been proposed [14], though evidence for infected immune cells remains scarce. However, neurological disorders are not limited to severe COVID-19 cases, suggesting that multiple brain entries may account for SARS-CoV-2 neurotropism. Although SARS-CoV-2 can enter the brain, experimental evidence of its presence in key brain regions involved in cognitive functions is still lacking, and little is known about the functional impact of SARS-CoV-2 CNS invasion on neurons.

SARS-CoV-2 entry into host cells is facilitated by its cell surface receptors. The spike proteins of both SARS-CoV-2 and the earlier SARS-CoV-1 bind to angiotensin-converting enzyme 2 (ACE2) as the first step of cellular entry [15]. The presence of ACE2 in neurons of the brain has been demonstrated [16]. However, ACE2 is expressed at relatively low levels in most tissues [17]. SARS-CoV-2 exhibits much higher infectivity than SARS-CoV-1. This evidence implicates either the existence of other cell surface receptors in SARS-CoV-2 cell entry or the facilitation of cell entry by other factors. Indeed, neuropilin-1 (NRP1) has been identified as a facilitator of SARS-CoV-2 entry when ACE2 is expressed, leading to high rates of infection [17]. NRP1 effectively binds to the protease furin-cleaved spike protein of SARS-CoV-2 [17], a process that does not occur for SARS-CoV-1. NRP1 is abundantly expressed in cells of many tissues including neurons [18]. The presence of ACE2 and NRP1 in neurons suggests the high possibility of neurotropism. It is of interest to determine in which cell types in the CNS and at which stage of neural development SARS-CoV-2 can exert its infectibility.

There is a profound link between SARS-CoV-2 infection and dementia/Alzheimer's disease. The 2002 and 2012 SARS and MERS epidemics caused memory impairment in many recovered patients [19]. Neurological syndromes related to Alzheimer's disease, including neuroinflammatory syndromes [20, 21], seizures [22], delirium [23, 24], and alterations in personality, behavior, and cognitive deficits [20, 25], frequently occur in patients with COVID-19 who recover from COVID-19. Thus, SARS-CoV-2 infection of the brain may increase the risk of Alzheimer's disease. The direct effects of SARS-CoV-2 on neuronal

function and survival, the inflammatory cytokine response, and hypoxia may lead to an Alzheimer's-like manifestation [26, 27]. Additionally, Alzheimer's patients have twice the risk of contracting COVID-19, which deteriorates Alzheimer's symptoms and increases mortality [28]. The cellular mechanism underlying the possible neurotropism of SARS-CoV-2 needs to be revealed for the development of possible treatments for a large number of COVID-19 survivors suffering from neurological disorders.

In this study, we sought to test whether SARS-CoV-2 is neurotropic and infects neural cells in the cognitive center in five patients with Alzheimer's disease, autism, frontotemporal dementia and no underlying condition, respectively. SARS-CoV-2 infection alters transcriptomic landscapes in favor of the development of Alzheimer's-like neuropathology in non-Alzheimer's individuals and exacerbates Alzheimer's neuropathology in patients with Alzheimer's. We found that SARS-CoV-2 invades the cognitive centers of all five COVID-19 patients, leading to Alzheimer's-like neuropathology or Alzheimer's neuropathology exacerbation. SARS-CoV-2 infects human inducible pluripotent stem cell (iPSC)-derived mature neurons from healthy individuals, leading to amyloid beta (Aβ) deposition, increased inflammation, neuronal death and increased expression of Alzheimer's mediators. Strikingly, we found that SARS-CoV-2-infects neurons from healthy individuals through a shared gene expression program with Alzheimer's neurons, leading to activation of the infectious pathways and supporting the infectious etiology of Alzheimer's disease.

Results

SARS-CoV-2 invades cognitive centers of the brain

Because ACE2, the SARS-CoV-2 cellular receptor, and NRP1, a facilitator of SARS-CoV-2 entry, are expressed in CNS neurons, we hypothesized that SARS-CoV-2 can infect neural cells in the brain, especially under conditions such as Alzheimer's disease and autism with BBB compromise. SARS-CoV-2 has been observed in cells of olfactory bulbs. We focused on cognitive centers of the brain. The SARS-CoV-2 spike protein and nucleocapsid protein were detected in cells of the inferior frontal cortexes of five COVID-19 cases: two autism cases, one Alzheimer's case, one frontotemporal dementia (FTD) case and one case without any underlying health conditions (apparently healthy case) (Fig. 1, Fig. S1). In contrast, there was no positive staining of spike protein or nucleocapsid protein in the cortexes of the non-COVID-19 autism brains (Fig. 1A, C, Fig. S1A). Spike protein- and nucleocapsid protein-positive viral particles were robustly present in the cytoplasm and cellular projections of cortical cells (Fig. 1E, F). RNAscope *in situ* hybridization detected the abundant presence of SARS-CoV-2 genomic RNA in cortical cells of the five COVID-19 cases (Fig. 1G, H; Fig. S1F). PCR analysis using the CDC method [29] confirmed the presence of SARS-CoV-2 RNA in the three cases that had frozen brain tissues (Fig. 1I). In the 31-year-old COVID-19 autism case, the amounts of SARS-CoV-2 RNA in the inferior frontal cortex and the dorsolateral prefrontal cortex were comparable to those in the lungs (Fig. 1I). In the COVID-19 FTD case and the COVID-19 apparently healthy case, SARS-CoV-2 RNA was also detected, whereas there was no SARS-CoV-2 RNA in the age-matched non-COVID-19 FTD individual or in the age-matched non-COVID-19 apparently healthy individual (Fig. 1I).

Additional analyses showed that cells of the three cortical regions, the entorhinal cortex, the inferior frontal cortex and the dorsolateral prefrontal cortex, in the two COVID-19 autism cases and the COVID-19 Alzheimer's case possessed abundant spike protein staining signals (Fig. 1J, K, L). The

numbers of SARS-CoV-2 spike protein-positive cells in these three regions were different in these three COVID-19 cases (Fig. 1J, K, L). These findings demonstrated that SARS-CoV-2 was neurotropic in this cohort of COVID-19 patients (Table S1).

SARS-CoV-2 infects CNS cells expressing ACE2 and NRP1

Because SARS-CoV-2 exists in cortical cells in COVID-19 patients, these cells must express ACE2 and NRP1. Indeed, the SARS-CoV-2 spike protein staining signal was colocalized with both ACE2 and NRP1 signals (Fig. 2A, B), indicating that SARS-CoV-2 infects cortical cells using these proteins. ACE2 was colocalized with the neuron marker neurofilament light chain (NFL) (Fig. 2C, D), the pan-neuron marker class III beta-tubulin (Tuj1) (Fig. 2E), the oligodendrocyte marker 2',3'-cyclic nucleotide-3'-phosphodiesterase (CNPase) (Fig. 2F), and the microglia marker ionized calcium-binding adapter molecule 1 (Iba1) (Fig. 2G). Quantitative analysis of double ACE2 and cell marker positive cells indicated that all neurons expressed ACE2 (Fig. 2H). Next, we determined which cell types in the cortexes were infected by SARS-CoV-2. We used dual immunohistological labeling with antibodies against cell type-specific markers and the SARS-CoV-2 spike protein. Both the mature neuron marker neuronal nuclear protein (NeuN) and the pan-neuron marker class III beta-tubulin (Tuj1) were colocalized with the spike protein in cells of the inferior frontal cortex (Fig. 2I, J). In the same region, both GABAergic inhibitory neurons (GAD65-positive) and glutamatergic excitatory neurons (glutamine synthetase-positive) contained SARS-CoV-2 spike protein staining signals (Fig. 2K, L). The SARS-CoV-2 spike protein staining signal was also present in Iba1-positive microglia and CNPase-positive oligodendrocytes in the same region (Fig. 2M, N). However, there was no detectable SARS-CoV-2 spike protein staining signal in glial fibrillary acidic protein (GFAP)-positive astrocytes (Fig. 2O). Quantification of double SARS-CoV-2 spike protein- and different cell type marker-positive cells indicated that spike protein was present in all neurons (Fig. 2P). Thus, SARS-CoV-2 infects various CNS cell types. Because infected peripheral

immune cells may enter the brain, T and B cells were examined in the inferior frontal cortex. There were no T, B cell, or macrophage marker staining signals in this region of the COVID-19 autism cases (Fig. S2). However, a significant number of these immune cells were detected in the COVID-19 Alzheimer's brain (Fig. S2).

SARS-CoV-2 causes cell death via multiple pathways

To determine whether SARS-CoV-2-infected cells in the cortical regions undergo cell death, we used immunohistological dual labeling with antibodies against the spike protein and cleaved caspase-3. There was no detectable cleaved caspase 3 staining signal in cells of the inferior frontal cortexes of non-COVID-19 autism controls (Fig. 3A). Over 90% of cleaved caspase 3-positive cells were SARS-CoV-2 spike protein positive in the cortexes of two COVID-19 autism cases (Fig. 3A). In the COVID-19 Alzheimer's disease case, over 20% of cleaved caspase 3-positive cells were SARS-CoV-2 spike protein positive (Fig. 3B). Cleaved caspase 3 was induced in two COVID-19 autism cases and the COVID-19 case without underlying health conditions and was enhanced in the COVID-19 Alzheimer's case and the COVID-19 FTD case (Fig. S3A, B, C).

To further determine the type of programmed cell death, we examined the presence of necroptotic, ferroptotic, and senescent cells. The cell necroptosis markers phospho-MLKL (mixed lineage kinase domain-like) and phospho-RIPK3 coexisted in spike protein-positive cells (Fig. 3C, Fig. S3D). Similarly, the two cell ferroptosis markers TfR1 (transferrin receptor) and ASCL4 (long-chain fatty acyl-CoA synthetase 4) were expressed in cells with positive spike protein signals (Fig. 3D, Fig. S3E). Because the cytokine associated with SARS-CoV-2 may trigger the cellular senescence program, we detected the senescence marker DPP4 (dipeptidyl-peptidase 4) in a subset of spike protein-positive cells (Fig. 3E). There were negligible double spike protein- and TfR1- or p-RIPK3-positive cells in the COVID-19 Alzheimer's case (Fig. 3D, Fig. S3D). These findings suggest that SARS-CoV-2 leads to cell death and

180 senescence through multiple pathways.

181 **SARS-CoV-2 induces neuroinflammation**

182 It has been suggested that SARS-CoV-2 infection leads to neuroinflammation. However, direct
183 evidence on the link between SARS-CoV-2 and neuroinflammation is still lacking. The protein expression
184 of two cytokines, IL-1β and IL-6 (interleukin 6), was significantly increased in the cortical cells of
185 COVID-19 autism patients compared to the cortical cells of non-COVID-19 autism patients (Fig. S4A, B,
186 C), providing the direct evidence of neuroinflammation induced by SARS-CoV-2.

187 **SARS-CoV-2 induces Alzheimer's-like phenotype development and exacerbation**

188 Cellular Aβ (amyloid beta) aggregates were observed in the cortexes of the two COVID-19 autism
189 cases (Fig. 4A) and the one COVID-19 case without underlying health conditions (Fig. 4B), whereas it
190 was not present in the cortexes of age-matched non-COVID-19 autism cases and an apparently healthy
191 individual (Fig. 4A, B). Extracellular Aβ plaques were present in one of the COVID-19 autism cases (Fig.
192 4A). Immunofluorescence analysis with thioflavin-T confirmed that the cytoplasmic deposition of Aβ in
193 the COVID-19 autism cases consisted of aggregated Aβ (Fig. 4A). There was more Aβ plaque deposition
194 per measured area in the cortexes of the COVID-19 Alzheimer's and FTD brains than in the cortexes of
195 age-matched non-COVID-19 Alzheimer's and FTD brains (Fig. 4C, D). One of the neuropathological
196 hallmarks of Alzheimer's disease is the development of intracellular neurofibrillary tangles (NFTs)
197 composed of hyperphosphorylated Tau (microtubule-associated protein tau). p-Tau-containing NFTs are
198 associated with neuronal dysfunction, cognitive deficits and neuronal death [30, 31]. p-Tau-containing
199 NFTs were present in the inferior cortexes of the two COVID-19 autism cases (Fig. 4E). Cellular p-Tau
200 deposition was induced in these two COVID-19 autism cases and the COVID-19 case without underlying
201 health conditions (Fig. 4E, F), whereas there were no signals or negligible p-Tau staining signals in the
202 cortexes of non-COVID-19 control brains (Fig. 4E, F). There were significantly higher numbers of Pick

bodies in the COVID-19 FTD case than in age-matched non-COVID-19 FTD cases (Fig. 4G, H). Thus, SARS-CoV-2 infection is linked to Alzheimer's neuropathology.

SARS-CoV-2 infects iPSC-derived mature neurons

Based on the above findings in neurons of COVID-19 patients' brain cortexes, we propose that SARS-CoV-2 can effectively infect neurons. To establish an *in vitro* platform to study this process, we obtained iPSCs derived from age-matched healthy individuals and Alzheimer's patients and differentiated it into neurons, followed by SARS-CoV-2 infection. SARS-CoV-2-GFP (in which GFP replaced the viral open reading frame ORF7a [32]) at a multiplicity of infection (MOI) of 0.1 or 0.2 did not infect any cells at iPSC neuron differentiation day 35 (Fig. 5A, Fig. S5A) and some of these cells expressed the pan-neuron marker Tuj1 but did not express the mature neuron marker NeuN (Fig. 5B, Fig. S5B). At iPSC differentiation day 50, SARS-CoV-2-GFP at an MOI of 0.05, 0.1 or 0.2 effectively infected cells differentiated from iPSCs from healthy individuals and Alzheimer's patients (Fig. 5C, Fig. S5C, D), and SARS-CoV-2-GFP could be detected in cell culture media 72 hours post SARS-CoV-2-GFP infection (Fig. 5D), indicating that the virus not only infects cells but also replicates intracellularly. SARS-CoV-2-infected cells were essentially all Tuj1-positive cells at iPSC differentiation day 50 (Fig. 5E), and no GFAT-positive astrocytes were detected in mock- and SARS-CoV-2-infected cells (Fig. 5F). At iPSC differentiation day 35, there was no expression of ACE2 or NRP1 proteins (Fig. 5G, H). At iPSC differentiation day 50, robust ACE2 and NRP1 protein expression existed in Tuj1-positive neurons (Fig. 5I, J). Over 40% of Tuj1-positive neurons were ACE2- and/or NRP1-positive (Fig. 5I, J). Subsequent experiments were conducted on iPSC differentiation day 50. These results suggest that SARS-CoV-2 infects mature neurons via ACE2 with the facilitation of NRP1.

SARS-CoV-2 induces Alzheimer's phenotypes in iPSC-derived cells

Because SARS-CoV-2 induces Aβ cellular aggregates and extracellular plaques, p-Tau cellular

deposition and NFTs and neuroinflammation in COVID-19 patients, we hypothesized that SARS-CoV-2 infection can turn neurons derived from iPSCs from healthy individuals into Alzheimer's-phenotype neurons. Neurons differentiated from iPSCs of healthy individuals and Alzheimer's patients were infected with wild-type SARS-CoV-2 (WA-1 strain [33]) at an MOI of 0.1 for 48 hours (Fig. 6, Fig. S6). SARS-CoV-2 induced cellular Aβ aggregates in healthy neurons and increased cellular Aβ aggregates in Alzheimer's neurons (Fig. 6A). Cellular p-Tau deposition was induced in healthy neurons after 72 hours of SARS-CoV-2 infection (Fig. 6B), and the virus further increased cellular p-Tau deposition in Alzheimer's neurons (Fig. 6B). Compared to their mock-infected counterparts, both healthy neurons and Alzheimer's neurons had higher levels of major inflammatory cytokines including IL-1β, IL-6, IFNγ and TNFα after SARS-CoV-2 infection (Fig. 6C). Among the critical Alzheimer's mediators, amyloid precursor protein (APP), enzyme β-secretase 1 (BACE1), and presenilin 1/2 (PSEN1/2), SARS-CoV-2 significantly increased BACE1 expression in healthy neurons and Alzheimer's neurons but did not affect the expression of the other Alzheimer's mediators (Fig. 6D, E). Likewise, SARS-CoV-2 significantly increased the number of cleaved caspase 3-positive cells differentiated from iPSCs of healthy individuals and Alzheimer's patients (Fig. 6F). Thus, SARS-CoV-2 triggers an Alzheimer's-like cellular program in neurons derived from iPSCs of healthy individuals and enhances Alzheimer's phenotypes in cells derived from Alzheimer's iPSCs.

Alzheimer's infectious etiology genes identified via SARS-CoV-2

Over 95% of Alzheimer's cases are sporadic and their causes are still unclear. Studies of DNA viruses have shown that Alzheimer's etiology has an infectious component [34, 35]. Based on the above observation that SARS-CoV-2 induces Alzheimer's phenotypes in neurons derived from iPSCs of healthy non-Alzheimer's individuals, we aimed to utilize SARS-CoV-2 infection to reveal genes responsible for the Alzheimer's infectious etiology. The transcriptomes of neurons differentiated from iPSCs of healthy

individuals and Alzheimer's patients were determined by RNA sequencing (Fig. 7A-E). Under mock infection conditions, 553 genes were significantly upregulated, while 71 genes were significantly downregulated, in Alzheimer's neurons compared to neurons from iPSCs of healthy individuals (designated healthy neurons) (Fig. 7A). SARS-CoV-2 upregulated 75 genes and downregulated 19 genes in healthy neurons (Fig. 7B). To extract the genes responsible for Alzheimer's infectious etiology, 24 overlapping genes were identified between the Alzheimer's neuron-mock-infected group and the healthy neuron-SARS-CoV-2-infected group (Fig. 7D). Pathway analysis revealed that the changes in these 24 genes activated infection pathways elicited by bacteria and viruses (Fig. 7D).

Compared to healthy neurons without viral infection, Alzheimer's neurons infected with SARS-CoV-2 had 517 upregulated genes and 256 downregulated genes (Fig. 7C). This number of downregulated genes (256) was higher than the number of downregulated genes in Alzheimer's neurons (71) (Fig. 7A, C). In Alzheimer's neurons, SARS-CoV-2 further increased the expression of 25 upregulated genes and decreased the expression of 34 downregulated genes by several-fold (Fig. S6A), indicating that the virus deteriorates Alzheimer's conditions, and pathway analysis pointed to the further activation of neuroinflammation and other processes in Alzheimer's neurons (Fig. S6B).

Top genes in the Alzheimer's infectious etiology transform neurons

The 24 overlapping genes between Alzheimer's neurons without SARS-CoV-2 infection and healthy neurons infected by SARS-CoV-2 are potential genes involved in the Alzheimer's infectious etiology. To evaluate whether the top upregulated genes among these 24 genes can turn healthy neurons into Alzheimer's-like neurons, we overexpressed the top three genes individually, FCGR3, LILRB5 and OTOR, in human primary neurons from a heathy individual. Overexpression of these genes in healthy neurons did not trigger cellular Aβ aggregation or cellular p-Tau deposition (Fig. S7D). In contrast, when the top three downregulated genes in the 24-gene list, GJA8, CryAA2 and PSG6, were individually

272 silenced in healthy human neurons, cellular expression of Aβ42 and p-Tau, cellular Aβ aggregation and
273 cellular p-Tau deposition were induced (Fig. 7F, Fig. S7E). Furthermore, silencing these top three
274 downregulated genes simultaneously in healthy human neurons robustly triggered cellular Aβ aggregation
275 and cellular p-Tau deposition (Fig. 7G). Thus, silencing the top three downregulated genes reprogrammed
276 healthy human neurons into Alzheimer's-like neurons.
277

Discussion

Although it is still controversial whether SARS-CoV-2 invades patients' brains [10, 36], we provide strong evidence that SARS-CoV-2 can invade the cognitive centers of the brain, leading to Alzheimer's-like phenotypes and exacerbation of Alzheimer's neuropathology. Examination revealed that iPSC-derived neurons infected by SARS-CoV-2 recapitulated the key aspects related to clinically observed neurological disorders in COVID-19 patients and survivors: neurotropism and Alzheimer's induction or enhancement by SARS-CoV-2.

Our observations from both COVID-19 autism and Alzheimer's brains support the effective infection of neurons, oligodendrocytes and other brain cells by SARS-CoV-2. Thus, the present study demonstrates the neurotropism of SARS-CoV-2. Such neurotropism has long been known to occur for other types of human respiratory coronaviruses [37]. Consistent with the current findings, in human iPSC-derived brain sphere neurons, SARS-CoV-2 at a dose equivalent to that in the present study has been found to not only infect neurons but also replicate itself in these neurons [38]. SARS-CoV-2 viral particles are present in both neuronal cell bodies and neurites [38]. SARS-CoV-2 can effectively infect cortical-like neurons in iPSC-derived brain organoids and these neurons express the SARS-CoV-2 receptor ACE2 and key coronavirus entry-associated proteases [39]. Regarding the infectibility of human brains by SARS-CoV-2, viral RNA has been detected in 36.4% of brain biopsies of fatal COVID-19 cases [9], suggesting that SARS-CoV-2 invades some COVID-19 patients' brains but may not invade all patients' brains. The current study examined cortical neurons of the brains of COVID-19 patients with either autism or Alzheimer's disease and observed full infectibility by SARS-CoV-2 in all cases. Similarly, a recent study using spike protein staining demonstrated that SARS-CoV-2 was present in some brain regions in all three COVID-19 cases studied [10]. Using multiple approaches, we showed the presence of spike and nucleocapsid proteins and SARS-CoV-2 viral particles in the cortical regions of all three COVID-19 cases

with either autism or Alzheimer's.

An early study showed no evidence of SARS-CoV-2 infection of neurons [40]. In iPSC-derived brain organoids, SARS-CoV-2 infects only mature choroid plexus cells, not neurons or glial cells [40]. This discrepancy may be due to the different developmental stages of neurons. We show that iPSC-derived immature neurons do not express ACE2 and NPR1 and thus are not able to be infected by SARS-CoV-2, whereas mature neurons do express these two SARS-CoV-2 receptors and are infected by this virus. Pellegrini et al. [40] did not observe ACE2 expression in neurons. In COVID-19 patients, not all neurons are infected by SARS-CoV-2 [10], suggesting that different types of neurons have differential expression of ACE2 and other SARS-CoV-2 entry factors and variable SARS-CoV-2 infectability. We and others [10] have shown that cortical neurons including excitatory and inhibitory neurons, are able to be infected by SARS-CoV-2.

SARS-CoV-2 enters hosts through their noses, mouths and eyes; thus, the anatomical proximity between the nasal cavity/nasopharynx and the olfactory mucosa may enable olfactory transmucosal entry of SARS-CoV-2 into the CNS [8]. The other major CNS entry route may depend on BBB leakage in conditions of autism and Alzheimer's disease [12, 13]. This may have been the case in our study, in which three COVID-19 patients had either autism or Alzheimer's disease. The BBB entry route is supported by a direct observation of BBB damage in COVID-19 patients [41]. Furthermore, the SARS-CoV-2 spike protein can disrupt human BBB integrity in 3D microfluidic *in-vitro* models [42]. The infiltration of infected immune cells into the brain has been proposed as a potential CNS entry route [14]. In agreement with a prior report, no sign of infected immune cell infiltration into COVID-19 autism patients' brains was found in the present study. Immune cells were present in the cortex in the COVID-19 Alzheimer's case. Thus, BBB leakage may be the major CNS entry route for SARS-CoV-2 into autism brains.

Apoptotic cell death is observed in the cells of brain organoids infected with SARS-CoV-2 [10, 39,

43, 44]. SARS-CoV-2-infected cells may not be very susceptible to apoptosis because the majority of cells undergoing apoptosis are noninfected but adjacent to SARS-CoV-2-positive cells [10]. The causes of apoptosis may be SARS-CoV-2-induced cellular inflammation and hypoxia, which occur in brain organoids infected by this virus [10, 43]. In COVID-19 patients, we found that apoptosis mostly occurred in cells infected by SARS-CoV-2. We found that cellular inflammation was induced in both iPSC-derived neurons and COVID-19 patient cortexes, suggesting that cellular inflammation is the primary factor leading to cell death. Other factors such as p-Tau, as detected by our group and others [44], may also play important roles in defining cell fates. SARS-CoV-2 infection induces not only apoptosis but also other nonapoptotic cell death programs, such as necroptosis and ferroptosis, as well as senescence [45], as observed in the current study. Thus, SARS-CoV-2 infection alters cellular programs, leading to critical cell mass loss and cellular dysfunction.

COVID-19 patients and survivors experience Alzheimer's-like neural syndrome including memory loss, delirium and cognitive deficits [25], suggesting that there is a cellular mechanism underlying these phenomena. A prior study showed altered distribution of Tau from axons to soma and Tau hyperphosphorylation in neurons of brain organoids exposed to SARS-CoV-2 [44]. We observed p-Tau tangles in the cortexes of two young autism COVID-19 patients, suggesting that neurodegenerative characteristics manifest in COVID-19 patients' brains. Aβ deposition and neuroinflammation were also present in the cognitive centers of these two young autism COVID-19 patients and in iPSC-derived neurons infected by SARS-CoV-2. These observations potentially explain the Alzheimer's-like brain disease observed in individuals exposed to SARS-CoV-2.

The pathogenesis of Alzheimer's disease contains an element of infectious disease pathogenesis. Pathogen infections can lead to the onset and progression of Alzheimer's disease. Insertions of viral DNA genomes into spontaneous late-onset Alzheimer's patient genomes have been determined [34]. Viral DNA

insertions in the host genome correlate with the induction of critical Alzheimer's mediators, such as enzymes involved in Aβ species production, aggregation and plaque formation [34]. Direct evidence for the involvement of viral DNA in Alzheimer's pathogenesis comes from the demonstration that herpes simplex virus type I (HSV-1) induces multicellular amyloid plaque–like structure formation, gliosis, and neuroinflammation in iPSC-derived neural cells and a 3D human brain-like model [35]. We provide direct evidence that the COVID-19 pandemic-causing virus SARS-CoV-2 triggers an Alzheimer's-like molecular program involving a group of 24 genes related to infectious disease pathway activation. The β-secretase BACE1, which produces all monomeric forms of amyloid-β (Aβ), including Aβ42, was induced by SARS-CoV-2 in iPSC-derived neurons from healthy individuals; thus, BACE1 may be a primary driver of the Alzheimer's-like phenotypes induced by SARS-CoV-2. SARS-CoV-2-induced hypoxia [10] may be responsible for BACE1 induction because hypoxia facilitates Alzheimer's pathogenesis by inducing BACE1 expression [46]. Because 26 of the 29 SARS-CoV-2 proteins physically associate with many proteins in human cells [47], it is also possible that one or some of the 29 SARS-CoV-2 proteins interact with transcriptional regulators in host cells, leading to BACE1 upregulation. The mechanism underlying SARS-CoV-2-induced Alzheimer's-like phenotypes needs to be further investigated.

In summary, we found that SARS-CoV-2 neurotropism exhibited full penetrance in the cortexes of COVID-19 autism and Alzheimer's patients. SARS-CoV-2 infection induced Alzheimer's-like phenotypes in autism patients and exacerbated neuropathology in Alzheimer's patients. SARS-CoV-2 infection triggered cellular and molecular Alzheimer's pathogenesis programs in iPSC-derived neurons from healthy individuals and enhanced neuropathological phenotypes in iPSC-derived neurons from Alzheimer's patients. We reveal a list of 24 genes that potentially mediate the infectious etiology of Alzheimer's disease under the condition of SARS-CoV-2 infection.

Acknowledgments

This work was supported by NIH grants R01HD100195, R01HD102206, R01HD099843, R01DK083243, R01DK101972, R01HL131737, R01HL134368, R01HL139060, R01DK103024 and P30-AG062429. No potential conflicts of interest relevant to this article are reported. The authors thank Jeffrey Metcalf, Sara Shuldberg and Sophia Perrott from the Rissman lab and UCSD Shiley-Marcos ADRC for technical assistance with this project.

Author Contributions

Shen WB, Penghua Yang, Montasir M, Xu C, Logue J, and Baracco L researched the data. Frieman M, Reece EA, Blanchard T, Li L, Han Z, and Rissman R analyzed the data and revised the manuscript. Peixin Yang conceived the project, designed the experiments, and wrote the manuscript. All authors approved the final version of the paper.

Declaration of Interests

The authors declare no competing interests.

Main figure titles and legends

Figure 1. SARS-CoV-2 is present in cortical cells in COVID-19 patients.

Representative images of SARS-CoV-2 spike protein staining in the inferior frontal cortexes of an age-matched non-COVID-19 autism (ASD) case (**A**) and a COVID-19 autism case (ID #6437) (**B**).

Representative images of SARS-CoV-2 nucleocapsid protein in the inferior frontal cortexes of an age-matched non-COVID-19 autism case (**C**) and a COVID-19 autism case (ID #6437) (**D**).

High-magnification imaging indicated that spike protein-positive (**E**) or nucleocapsid protein-positive (**F**) viral particles were located in both the cytoplasm and cellular processes (arrows).

SARS-CoV-2 genomic RNA was detected by RNAscope in the cortical cells of the COVID-19 autism case (**H,** arrows) but not in the age-matched non-COVID-19 autism case (**G**).

COVID-19 PCR test revealed SARS-CoV-2 positivity in brain regions of two COVID-19 cases along with lung positivity (ID #6436) (**I**). Red * indicates nonspecific bands compared to the 72 bp positive band. Melt curve analysis and DNA sequencing of PCR products confirmed SARS-CoV-2 positivity in brain tissues.

SARS-CoV-2 spike protein staining positivity in the EC, IFC and DPC in the COVID-19 Alzheimer's case (ID #6435) (**J**) and in COVID-19 autism case 1 (ID #6436) (**K**) and case 2 (ID #6437) (**L**). The spike protein-positive cells per mm^2 were quantified in the three brain regions. Cells were counted from at least 3 sections ($n \geq 3$). EC: Entorhinal cortex; IFC: inferior frontal cortex; DPC: dorsolateral prefrontal cortex. Scale bars: A-D, J-L = 20 μm; E, F = 10 μm; G, H = 5μm. * indicate significant difference ($P < 0.05$) by one-way ANOVA and *Tukey* test.

Figure 2. hACE2-positive or neuropilin 1 (NRP1)-positive neurons and nonneuronal cells exhibit SARS-CoV-2 positivity.

(**A**) Double spike protein (SP, Ni-DAB: black signals)- and hACE2 (AP staining: red signals)-positive

409 cells in the inferior frontal cortexes (IFCs) of the COVID-19 autism cases, the COVID-19 Alzheimer's
410 case and their age-matched control cases: non-COVID-19 autism control cases and non-COVID-19
411 Alzheimer's cases. The graphs show the percentages of double positive cells among total hACE2 positive
412 cells in $n \geq 5$ random fields.
413 (**B**) Double SP (Ni-DAB: black signals)- and NRP1 (AP staining: red signals)-positive cells in the inferior
414 frontal cortexes of the COVID-19 autism cases, the COVID-19 Alzheimer's case and their age-matched
415 control cases. The graphs show the percentages of double positive cells among total NRP1-positive cells
416 in $n \geq 5$ random fields.
417 (**C**) Controls for immunohistological staining with normal IgG for Ni-DAB staining, AP staining or both
418 in the inferior frontal cortexes (IFCs) of non-COVID-19 autism cases and with an hACE2 antibody for
419 Ni-DAB staining.
420 Detection of the hACE2 receptor in neurons and nonneuronal cells in the IFCs of non-COVID-19 autism
421 cases. The hACE2-positive neurons are labeled with antibodies against NFL (**D**) or Tuj1 (**E**), the
422 oligodendrocyte marker CNPase (**F**), and the microglial marker Iba1 (**G**).
423 (**H**) hACE2 and cell marker double-positive cells were quantified (%, $n \geq 5$ random fields).
424 SP positivity was detected in neurons and nonneuronal cells in the IFCs of the COVID-19 autism case (ID
425 #6437). SP-positive neurons labeled with Tuj1 (**I**), NeuN (**J**), the GABAergic inhibitory neuronal marker
426 GAD65 (**K**), the glutamatergic excitatory neuronal marker GS (glutamine synthetase) (**L**), the
427 oligodendrocyte marker CNPase (**M**), and the microglial marker Iba1 (**N**). $GFAP^+$ astrocytes were SP
428 negative (green arrows) (**O**).
429 (**P**) Quantification of SP and cell marker double positive cells (%, $n \geq 5$ random fields).
430 AD: Alzheimer's disease; ASD: autism. Scale bar = 20 μm. In A and B, * indicate significant difference
431 ($P < 0.05$) by *t* test.

Figure 3. Spike protein-positive cells undergo programmed cell death.

Representative images of double SARS-CoV-2 spike protein (SP) (Ni-DAB staining: black signal) and cleaved caspase 3 (cl-casp3; AP: red signal) staining in the cortexes of age-matched non-COVID-19 autism and COVID-19 autism cases (**A**) and non-COVID-19 Alzheimer's and the COVID-19 Alzheimer's case (**B**). The inset boxes show cl-casp3 and SP double-labeled cells, cl-casp3-positive cells and double-negative cells.

The graphs show the percentages of double SP^+ and cl-$casp3^+$ cells among total cleaved $caspase\ 3^+$ cells in at least 5 random fields. * indicate significant difference ($P < 0.05$) compared with the non-COVID-19 controls by *t* test.

Representative images of SP staining with the necroptosis marker phospho-MLKL (**C**), the ferroptosis marker TfR1 (**D**), and the senescence marker DPP4 (**E**) in the cortexes of the non-COVID-19 autism cases, the COVID-19 Alzheimer's case and the two COVID-19 autism cases. Black arrows point to the double SP^+ and cl-$casp3^+$ cells.

The graphs show the percentages of SP^+ necroptotic cells, ferroptotic cells and senescent cells counted from at least 5 random fields ($n \geq 5$, in 2 COVID-19 ASD cases and 1 COVID-19 AD case). * indicate significant difference ($P < 0.05$) compared with the non-COVID-19 controls by one-way ANOVA and *Tukey* test. Scale bars = 20 μm.

Figure 4. SARS-CoV-2 infection induces or enhances Aβ aggregate/plaque and p-Tau pretangles formation.

Aβ immunohistochemical staining (with the anti-Aβ antibody 6E10) in three cortical regions of two cases of COVID-19 autism (**A**) and one case of COVID-19 with no underlying conditions (NUC) (**B**) and their age-matched control cases. Cytoplasmic deposition of Aβ (blue arrows) was observed in COVID-19

autism (ASD) cortexes, and Aβ plaques (red arrow) were observed in the EC of one COVID-19 ASD case. Immunofluorescence analysis with thioflavin-T indicated that the cytoplasmic deposits of Aβ in the COVID-19 autism cortex consisted of aggregated Aβ (inset in **A,** upper panel most right). (**C**) Aβ immunohistochemical staining in the cortical regions and hippocampi of the COVID-19 FTD and Alzheimer's disease cases, and their age-matched controls. (**D**) Quantification of cellular Aβ aggregates in ASD and NUC cases or Aβ plaques per mm^2 in FTD and AD cases (3 sections for each region and 3 independent images for one section). (**E**) p-Tau (pSer202) staining in the cortexes of COVID-19 ASD (E) and COVID-19 NUC (**F**) cases and their age-matched controls. (**G**) p-Tau staining in the cortexes and hippocampi of the two COVID-19 FTD and Alzheimer's disease cases and their age-matched controls. (**H**) Quantification of cellular p-Tau deposition per mm^2 (3 sections for each region and 3 independent images for one section). The two COVID-19 ASD cases showed p-Tau pretangle-like structures (indicated by red arrows) and cytoplasmic p-Tau deposition (indicated by blue arrows). Increased/elevated Pick body (red arrows) deposition was observed in the COVID-19 FTD case, and there were no differences in p-Tau tangle numbers in AD cases. Entorhinal cortex: EC; inferior frontal cortex: IFC; dorsolateral prefrontal cortex: DPC. Significant *P*-values are indicated (by Mann-Whitney U test after confirming a normal distribution). Bars = 100 μm.

Figure 5. SARS-CoV-2 infects mature neurons derived from human iPSCs.

(**A**). SARS-CoV-2-GFP does not infect immature neurons at iPSC neuron differentiation day 35 (n = 3 replicates).

(**B**). Immature neurons do not express the mature neuron marker, NeuN.

(**C**). SARS-CoV-2 infects mature neurons at iPSC neuron differentiation day 50 (n = 3).

(**D**). Detection of SARS-CoV-2 in the culture medium of infected neurons (n = 3).

(**E**). SARS-CoV-2 infects Tuj1-positive neurons (n = 3).

(**F**). GFAP is not expressed in SARS-CoV-2-infected cells at iPSC differentiation day 50 (n = 2).

Immature Tuj1-positive neurons do not express ACE2 (**G**) and NRP1 (**H**) (n = 3).

Mature Tuj1 positive neurons express ACE2 (**I**) and NRP1 (**J**) (n = 3).

The bar graphs show the percentages of double Tuj1- and ACE2- or NRP1-positive cells (yellow) among total $Tuj1^{+}$ cells (green) (n = 3). AD: Alzheimer's disease; CTL: control group (non-AD); ACE2: angiotensin-converting enzyme 2; Tuj1: beta-Tubulin III; NRP1: Neuropilin 1; SPIKE: SARS-CoV-2 spike protein.

Figure 6. SARS-CoV-2 induces or enhances Alzheimer's-like neuron phenotypes.

(**A**). SARS-CoV-2 induces cellular Aβ aggregation in neurons derived from iPSCs of healthy individuals and Alzheimer's patients (n = 3 iPSC lines).

(**B**). SARS-CoV-2 induces cellular p-Tau deposition in neurons derived from iPSCs of healthy individuals and Alzheimer's patients (n = 3 iPSC lines).

The values in the graphs are presented as the means ± SEMs (n = 5 images from 2 independent experiments for each group). The Aβ and p-Tau intensity data were analyzed by Mann-Whitney U test after confirming a normal distribution. Bars = 50 μm.

mRNAs levels of inflammatory cytokines (**C**), BACE1 (**D**), and Alzheimer's molecular mediators (APP, PSEN1 and PSEN2) (**E**) in SARS-CoV-2-infected neurons derived from iPSCs (n = 6, 3 iPSC lines for 2 independent experiments).

F. Cleaved caspase 3 (c-Cas3)-positive cells in SARS-CoV-2 infected neurons derived from iPSCs (n = 6 iPSC lines for 2 independent experiments). The bar graph shows the quantification of c-Cas3-positive cell numbers. CTL: control group (iPSCs from healthy individuals); AD: Alzheimer's disease; CTLv: SARS-CoV-2-infected control group; ADv: SARS-CoV-2-infected AD group; Tuj1: beta-Tubulin III; c-Cas3, cleaved caspase 3. Data were analyzed by Mann-Whitney U test after confirming a normal distribution,

501 significant *P*-values are presented.

502 **Figure 7. Identification of an infectious etiology gene signature for Alzheimer's disease.**

503 (**A**). Volcano plot of differentially expressed genes (DEGs) in neurons derived from iPSCs of patients with
504 Alzheimer's disease (AD) (the AD group) compared to neurons derived from iPSCs of healthy individuals
505 (the CTL group).

506 (**B**). Volcano plot of DEGs in healthy individual iPSC-derived neurons infected with SARS-CoV-2 (the
507 CTL_V group) compared to the CTL group.

508 (**C**). Volcano plot of DEGs in AD neurons infected with SARS-CoV-2 (the AD_V group) compared to the
509 CTL group.

510 (**D**). Venn plot and KEGG pathway analysis for DEGs between the AD group and the CTL_V group. The
511 CTL group served as the baseline group. The twenty-four overlapping genes constituted the AD infectious
512 etiology gene signature.

513 (**E**). Venn plot and KEGG pathway analysis for DEGs between the AD group and the AD_V group. The
514 CTL group served as the baseline group.

515 For **A** to **E**, n = 3 iPSC lines for the CTL and AD groups.

516 (**F-G**). Analysis of the effect of siRNA mediated individual or combined knockdown of the top 3
517 downregulated genes, GJA8, CryAA2 and PSG6, on the AD infectious etiology gene signature in primary
518 human neurons. **F**: Immunoblot analysis of Aβ isoforms (n = 3 replicates). **G**. Cellular Aβ aggregation
519 (left panel) and cellular p-Tau deposition (right panel). Aβ aggregates and p-Tau accumulation in the
520 cytoplasm or neuronal axon are indicated by white arrowheads. The values in the graphs are presented as
521 the means ± SEMs (n = 8 images from 3 replicates). Intensity data were analyzed by Mann-Whitney U
522 test after confirming a normal distribution, significant *P*-values are presented. Scale bar, 50 μm.

523

Supplemental figure titles and legends

Fig. S1. Presence of SARS-CoV-2 spike protein in cortical cells of five COVID-19 cases.

Spike protein staining signals were visualized with an alkaline phosphatase (AP)-coupled goat anti-rabbit secondary antibody and AP red substrate. SARS-CoV-2 spike protein red signals were located in the cytosol of cortical cells of one COVID-19 autism (ASD) case but not in cells of an age-matched non-COVID-19 ASD control (**A**). Spike protein (DAB staining, brown signal; counterstained with hematoxylin, blue) was present in the cytosol of cortical cells of the COVID-19 FTD case (ID #5922) (**C**, three different fields, arrows) but not in those of the age-matched non-COVID-19 FTD controls (**B,** 3 cases). In the COVID-19 case without underlying conditions (ID #5932), the spike protein was also visible (**E,** three different fields, arrows), but it was not visible in the age-matched non-COVID-19 AD controls (**D,** 3 cases). RNAscope *in situ* hybridization showing COVID-19 genomic RNAs in four COVID-19 cases (**F**): 2 ASD COVID-19 cases, 1 AD COVID-19 case, 1 FTD COVID-19 case, and 1 COVID-19 case without underlying conditions. Scale bar = 20 μm.

Fig. S2. Immunostaining of immune cell markers in brain tissues of COVID-19 patients.

Immunolabeling (DAB, brown signal) with antibodies against CD3 (T cell marker, **A**), CD20 (B cell marker, **B**), and F4/80 (macrophage marker, **C**) showed positively labeled immune cells in the cortex of the COVID-19 Alzheimer's case. Immune cells were not detected in non-COVID-19 autism cases or the two COVID-19 autism cases (**A-C**). Counterstaining: hematoxylin. The arrows point to immune cells. (**D**) The percentages of immune cells were quantified from 3 sections (n = 3). * indicates a significant difference ($P < 0.05$) by one-way ANOVA and Tukey's test. Scale bar = 20 μm.

Fig. S3. Programmed cell death in SARS-CoV-2 spike protein positive-cortical cells.

Representative images of cleaved caspase-3 staining (DAB, brown signal) in the cortexes of age-matched

548 non-COVID-19 autism cases, 2 COVID-19 autism cases, and 1 COVID-19 case with no underlying
549 conditions (**A**). Cleaved caspase-3-positive cells in the non-COVID-19 Alzheimer's, COVID-19
550 Alzheimer's, non-COVID-19 FTD, and COVID-19 FTD cases (**B**). Counterstaining: hematoxylin (blue).
551 (**C**) Quantification of cleaved caspase-3^+ cells in at least 5 random fields ($n \geq 5$, in 2 autism cases, 1 AD
552 case, 1 FTD case and 1 case without underlying conditions). The arrows point to cleaved caspase-3^+ (cl-
553 casp-3^+) cells. Representative images of spike protein-positive signals (black dots) with p-Ripk3^+
554 necroptotic cells (**D**) and ASCL4^+ ferroptotic cells (**E**) in the non-COVID-19, COVID-19 Alzheimer's
555 (AD), and COVID-19 autism (ASD) cases. The arrows point to the double-positive cells. Quantification
556 of double-positive cell numbers (spike protein and programmed cell death marker positive) from at least
557 5 random fields ($n \geq 5$). * indicates a significant difference ($P < 0.05$) compared with non-COVID-19
558 controls by one-way ANOVA and *Tukey's* test. Scale bar = 20 μm.
559
560 **Figure. S4. Cytokine expression in COVID-19 autism cortexes.**
561 Representative images of immunostaining of the cytokines IL-1β (**A**) and IL-6 (**B**) in the two cases of
562 COVID-19 autism (ASD) and in age-matched non-COVID-19 ASD controls (CTL) in the entorhinal
563 cortex (EC). (**C**) Quantification of immunostaining intensity (n = 6, 3 random fields per case per region).
564 Data were analyzed by Mann-Whitney U test after confirming a normal distribution, a significant *P*-value
565 is presented. Scale bar = 100 μm.
566
567 **Fig. S5. SARS-CoV-2 infects mature neurons derived from human iPSCs.**
568 (**A**) SARS-CoV-2-GFP does not infect immature neurons at iPSC differentiation day 35. White asterisks
569 (*) indicate nonspecific fluorescent signals. (**B**) Immature neurons do not express the mature neuron
570 marker NeuN. (**C**). SARS-CoV-2 infects mature neurons at iPSC differentiation day 50. (**D**). SARS-CoV-
571 2-GFP infects mature neurons at different dosages. CTL (non-AD: iPSCs derived from healthy

572 individuals): control groups; AD: Alzheimer's disease; Tuj1: beta-Tubulin III; SPIKE: SARS-CoV-2 spike
573 protein.
574
575 **Fig. S6. Effects of identified Alzheimer's infectious etiology genes on Aβ and p-Tau in human**
576 **primary neurons.** (**A**). Upregulated genes in AD neurons that were further upregulated due to SARS-
577 CoV-2 infection. (**B**). Downregulated genes in AD neurons that were further downregulated due to SARS-
578 CoV-2. (**C**). KEGG pathway analysis of the upregulated and downregulated genes in AD neurons that
579 were further upregulated and downregulated by SARS-CoV-2. CTL (non-AD: iPSCs derived from healthy
580 individuals): control groups; AD: Alzheimer's disease; ADV: SARS-CoV-2-infected AD group. For each
581 group, n = 3.
582 (**D**) Immunofluorescence staining with the indicated antibodies after lentivirus-mediated overexpression
583 of the top 3 upregulated genes, FCGR, LILRB5 and OTOR, identified in Fig. 7D as AD infectious etiology
584 genes. Combined or individual overexpression of these three genes did not induce Aβ cellular aggregation,
585 and only FCGR overexpression increased Tau phosphorylation at Ser202.
586 (**E**) Immunofluorescence staining of the indicated antibodies after siRNA-mediated knockdown of the top
587 3 downregulated genes, GJA8, CryAA2 and PSG6, identified in Fig. 7D as AD infectious etiology genes.
588 Knockdown of GJA8, CryAA2 or PSG6 individually caused Aβ cellular aggregation and significantly
589 increased Tau phosphorylation at Ser202.
590

References

[1] Helms J, Kremer S, Merdji H, Clere-Jehl R, Schenck M, Kummerlen C, et al. Neurologic Features in Severe SARS-CoV-2 Infection. N Engl J Med. 2020;382:2268-70.

[2] Mao L, Jin H, Wang M, Hu Y, Chen S, He Q, et al. Neurologic Manifestations of Hospitalized Patients With Coronavirus Disease 2019 in Wuhan, China. JAMA Neurol. 2020;77:683-90.

[3] de Erausquin GA, Snyder H, Carrillo M, Hosseini AA, Brugha TS, Seshadri S, et al. The chronic neuropsychiatric sequelae of COVID-19: The need for a prospective study of viral impact on brain functioning. Alzheimers Dement. 2021.

[4] Taquet M, Geddes JR, Husain M, Luciano S, Harrison PJ. 6-month neurological and psychiatric outcomes in 236 379 survivors of COVID-19: a retrospective cohort study using electronic health records. Lancet Psychiatry. 2021;8:416-27.

[5] De Santis G. SARS-CoV-2: A new virus but a familiar inflammation brain pattern. Brain Behav Immun. 2020;87:95-6.

[6] Li K, Wohlford-Lenane C, Perlman S, Zhao J, Jewell AK, Reznikov LR, et al. Middle East Respiratory Syndrome Coronavirus Causes Multiple Organ Damage and Lethal Disease in Mice Transgenic for Human Dipeptidyl Peptidase 4. J Infect Dis. 2016;213:712-22.

[7] Netland J, Meyerholz DK, Moore S, Cassell M, Perlman S. Severe acute respiratory syndrome coronavirus infection causes neuronal death in the absence of encephalitis in mice transgenic for human ACE2. J Virol. 2008;82:7264-75.

[8] Meinhardt J, Radke J, Dittmayer C, Franz J, Thomas C, Mothes R, et al. Olfactory transmucosal SARS-CoV-2 invasion as a port of central nervous system entry in individuals with COVID-19. Nat Neurosci. 2021;24:168-75.

[9] Puelles VG, Lutgehetmann M, Lindenmeyer MT, Sperhake JP, Wong MN, Allweiss L, et al. Multiorgan and Renal Tropism of SARS-CoV-2. N Engl J Med. 2020;383:590-2.

[10] Song E, Zhang C, Israelow B, Lu-Culligan A, Prado AV, Skriabine S, et al. Neuroinvasion of SARS-CoV-2 in human and mouse brain. J Exp Med. 2021;218.

[11] Zheng J, Wong LR, Li K, Verma AK, Ortiz ME, Wohlford-Lenane C, et al. COVID-19 treatments and pathogenesis including anosmia in K18-hACE2 mice. Nature. 2021;589:603-7.

[12] Montagne A, Zhao Z, Zlokovic BV. Alzheimer's disease: A matter of blood-brain barrier dysfunction? J Exp Med. 2017;214:3151-69.

[13] Fiorentino M, Sapone A, Senger S, Camhi SS, Kadzielski SM, Buie TM, et al. Blood-brain barrier and intestinal epithelial barrier alterations in autism spectrum disorders. Mol Autism. 2016;7:49.

[14] Iadecola C, Anrather J, Kamel H. Effects of COVID-19 on the Nervous System. Cell. 2020;183:16-27 e1.

[15] Hoffmann M, Kleine-Weber H, Schroeder S, Kruger N, Herrler T, Erichsen S, et al. SARS-CoV-2 Cell Entry Depends on ACE2 and TMPRSS2 and Is Blocked by a Clinically Proven Protease Inhibitor. Cell. 2020;181:271-80 e8.

[16] Butowt R, Bilinska K. SARS-CoV-2: Olfaction, Brain Infection, and the Urgent Need for Clinical Samples Allowing Earlier Virus Detection. ACS Chem Neurosci. 2020;11:1200-3.

[17] Cantuti-Castelvetri L, Ojha R, Pedro LD, Djannatian M, Franz J, Kuivanen S, et al. Neuropilin-1 facilitates SARS-CoV-2 cell entry and infectivity. Science. 2020;370:856-60.

[18] Vanacker C, Trova S, Shruti S, Casoni F, Messina A, Croizier S, et al. Neuropilin-1 expression in GnRH neurons regulates prepubertal weight gain and sexual attraction. EMBO J. 2020;39:e104633.

[19] Rogers JP, Chesney E, Oliver D, Pollak TA, McGuire P, Fusar-Poli P, et al. Psychiatric and neuropsychiatric presentations associated with severe coronavirus infections: a systematic review and meta-analysis with comparison to the COVID-19 pandemic. Lancet Psychiatry. 2020;7:611-27.

[20] Varatharaj A, Thomas N, Ellul MA, Davies NWS, Pollak TA, Tenorio EL, et al. Neurological and neuropsychiatric complications of COVID-19 in 153 patients: a UK-wide surveillance study. Lancet Psychiatry. 2020;7:875-82.

[21] Paterson RW, Brown RL, Benjamin L, Nortley R, Wiethoff S, Bharucha T, et al. The emerging spectrum of COVID-19 neurology: clinical, radiological and laboratory findings. Brain. 2020;143:3104-20.

[22] Kadono Y, Nakamura Y, Ogawa Y, Yamamoto S, Kajikawa R, Nakajima Y, et al. A case of COVID-19 infection presenting with a seizure following severe brain edema. Seizure. 2020;80:53-5.

[23] Hosseini AA, Shetty AK, Sprigg N, Auer DP, Constantinescu CS. Delirium as a presenting feature in COVID-19: Neuroinvasive infection or autoimmune encephalopathy? Brain Behav Immun. 2020;88:68-70.
[24] Alkeridy WA, Almaghlouth I, Alrashed R, Alayed K, Binkhamis K, Alsharidi A, et al. A Unique Presentation of Delirium in a Patient with Otherwise Asymptomatic COVID-19. J Am Geriatr Soc. 2020;68:1382-4.
[25] Jaywant A, Vanderlind WM, Alexopoulos GS, Fridman CB, Perlis RH, Gunning FM. Frequency and profile of objective cognitive deficits in hospitalized patients recovering from COVID-19. Neuropsychopharmacology. 2021.
[26] Heneka MT, Golenbock D, Latz E, Morgan D, Brown R. Immediate and long-term consequences of COVID-19 infections for the development of neurological disease. Alzheimers Res Ther. 2020;12:69.
[27] Vallamkondu J, John A, Wani WY, Ramadevi SP, Jella KK, Reddy PH, et al. SARS-CoV-2 pathophysiology and assessment of coronaviruses in CNS diseases with a focus on therapeutic targets. Biochim Biophys Acta Mol Basis Dis. 2020;1866:165889.
[28] Wang Q, Davis PB, Gurney ME, Xu R. COVID-19 and dementia: Analyses of risk, disparity, and outcomes from electronic health records in the US. Alzheimers Dement. 2021.
[29] Coil DA, Albertson T, Banerjee S, Brennan G, Campbell AJ, Cohen SH, et al. SARS-CoV-2 detection and genomic sequencing from hospital surface samples collected at UC Davis. PLoS One. 2021;16:e0253578.
[30] Gomez-Isla T, Hollister R, West H, Mui S, Growdon JH, Petersen RC, et al. Neuronal loss correlates with but exceeds neurofibrillary tangles in Alzheimer's disease. Ann Neurol. 1997;41:17-24.
[31] Giannakopoulos P, Herrmann FR, Bussiere T, Bouras C, Kovari E, Perl DP, et al. Tangle and neuron numbers, but not amyloid load, predict cognitive status in Alzheimer's disease. Neurology. 2003;60:1495-500.
[32] Hou YJ, Okuda K, Edwards CE, Martinez DR, Asakura T, Dinnon KH, 3rd, et al. SARS-CoV-2 Reverse Genetics Reveals a Variable Infection Gradient in the Respiratory Tract. Cell. 2020;182:429-46 e14.
[33] Tian JH, Patel N, Haupt R, Zhou H, Weston S, Hammond H, et al. SARS-CoV-2 spike glycoprotein vaccine candidate NVX-CoV2373 immunogenicity in baboons and protection in mice. Nat Commun. 2021;12:372.
[34] Readhead B, Haure-Mirande JV, Funk CC, Richards MA, Shannon P, Haroutunian V, et al. Multiscale Analysis of Independent Alzheimer's Cohorts Finds Disruption of Molecular, Genetic, and Clinical Networks by Human Herpesvirus. Neuron. 2018;99:64-82 e7.
[35] Cairns DM, Rouleau N, Parker RN, Walsh KG, Gehrke L, Kaplan DL. A 3D human brain-like tissue model of herpes-induced Alzheimer's disease. Sci Adv. 2020;6:eaay8828.
[36] Thakur KT, Miller EH, Glendinning MD, Al-Dalahmah O, Banu MA, Boehme AK, et al. COVID-19 neuropathology at Columbia University Irving Medical Center/New York Presbyterian Hospital. Brain. 2021.
[37] Arbour N, Day R, Newcombe J, Talbot PJ. Neuroinvasion by human respiratory coronaviruses. J Virol. 2000;74:8913-21.
[38] Bullen CK, Hogberg HT, Bahadirli-Talbott A, Bishai WR, Hartung T, Keuthan C, et al. Infectability of human BrainSphere neurons suggests neurotropism of SARS-CoV-2. ALTEX. 2020;37:665-71.
[39] Zhang BZ, Chu H, Han S, Shuai H, Deng J, Hu YF, et al. SARS-CoV-2 infects human neural progenitor cells and brain organoids. Cell Res. 2020;30:928-31.
[40] Pellegrini L, Albecka A, Mallery DL, Kellner MJ, Paul D, Carter AP, et al. SARS-CoV-2 Infects the Brain Choroid Plexus and Disrupts the Blood-CSF Barrier in Human Brain Organoids. Cell Stem Cell. 2020;27:951-61 e5.
[41] Alexopoulos H, Magira E, Bitzogli K, Kafasi N, Vlachoyiannopoulos P, Tzioufas A, et al. Anti-SARS-CoV-2 antibodies in the CSF, blood-brain barrier dysfunction, and neurological outcome: Studies in 8 stuporous and comatose patients. Neurol Neuroimmunol Neuroinflamm. 2020;7.
[42] Buzhdygan TP, DeOre BJ, Baldwin-Leclair A, Bullock TA, McGary HM, Khan JA, et al. The SARS-CoV-2 spike protein alters barrier function in 2D static and 3D microfluidic in-vitro models of the human blood-brain barrier. Neurobiol Dis. 2020;146:105131.
[43] Jacob F, Pather SR, Huang WK, Zhang F, Wong SZH, Zhou H, et al. Human Pluripotent Stem Cell-Derived Neural Cells and Brain Organoids Reveal SARS-CoV-2 Neurotropism Predominates in Choroid Plexus Epithelium. Cell Stem Cell. 2020;27:937-50 e9.

682 [44] Ramani A, Muller L, Ostermann PN, Gabriel E, Abida-Islam P, Muller-Schiffmann A, et al. SARS-CoV-2 targets neurons
683 of 3D human brain organoids. EMBO J. 2020;39:e106230.
684 [45] Lee S, Yu Y, Trimpert J, Benthani F, Mairhofer M, Richter-Pechanska P, et al. Virus-induced senescence is driver and
685 therapeutic target in COVID-19. Nature. 2021.
686 [46] Sun X, He G, Qing H, Zhou W, Dobie F, Cai F, et al. Hypoxia facilitates Alzheimer's disease pathogenesis by up-regulating
687 BACE1 gene expression. Proc Natl Acad Sci U S A. 2006;103:18727-32.
688 [47] Gordon DE, Jang GM, Bouhaddou M, Xu J, Obernier K, White KM, et al. A SARS-CoV-2 protein interaction map reveals
689 targets for drug repurposing. Nature. 2020;583:459-68.

690

Fig. 1

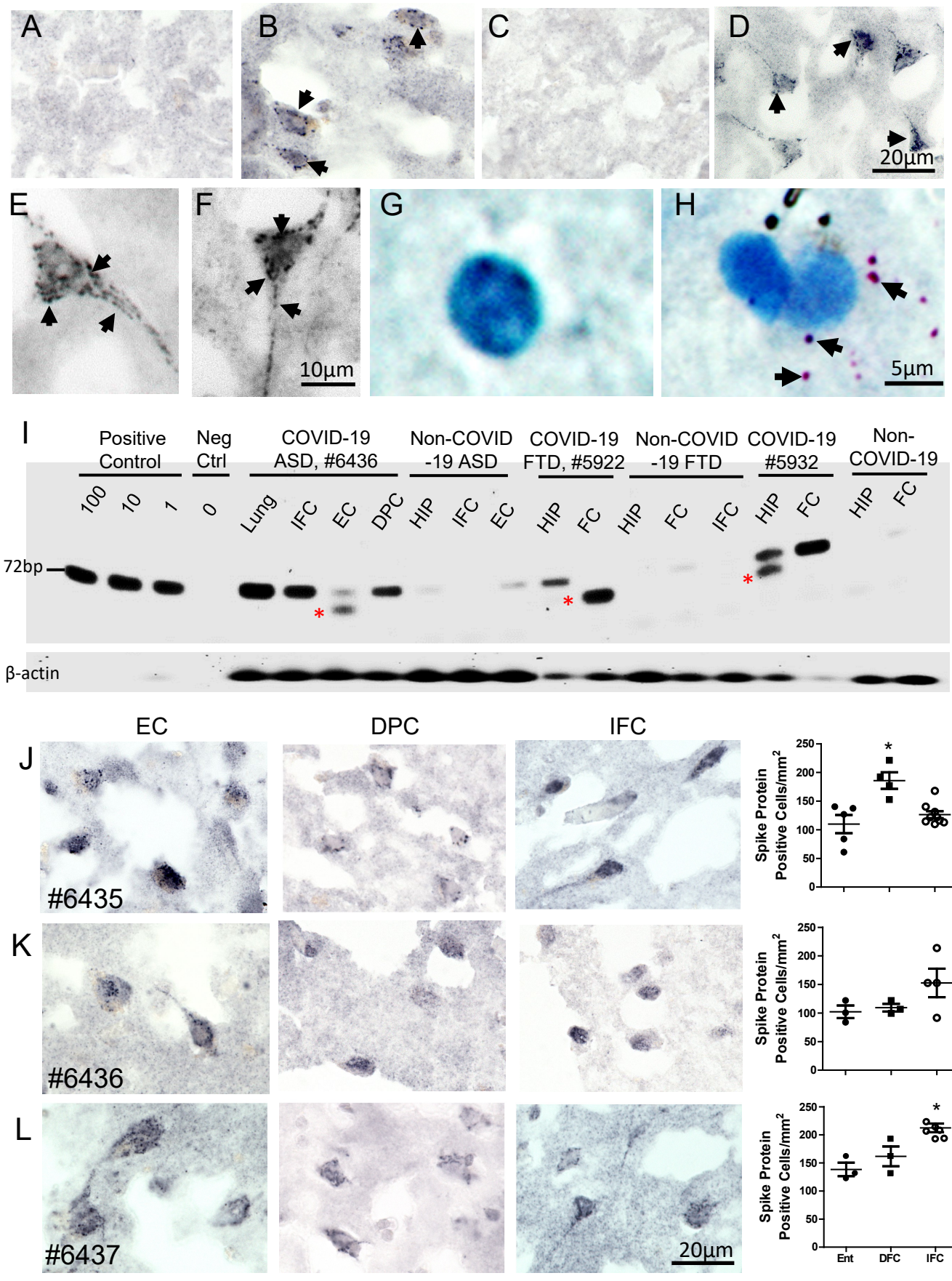
A
B
C
D
20µm
E
F
10µm
G
H
5µm
I
Positive Control
Neg Ctrl
COVID-19 ASD, #6436
Non-COVID -19 ASD
COVID-19 FTD, #5922
Non-COVID -19 FTD
COVID-19 #5932
Non-COVID-19
100
10
1
0
Lung
IFC
EC
DPC
HIP
IFC
EC
HIP
FC
HIP
FC
IFC
HIP
FC
HIP
FC
72bp
β-actin
EC
DPC
IFC
J
#6435
K
#6436
L
#6437
20µm
Spike Protein Positive Cells/mm2
250
200
150
100
50
0
Ent
DFC
IFC

Fig. 2

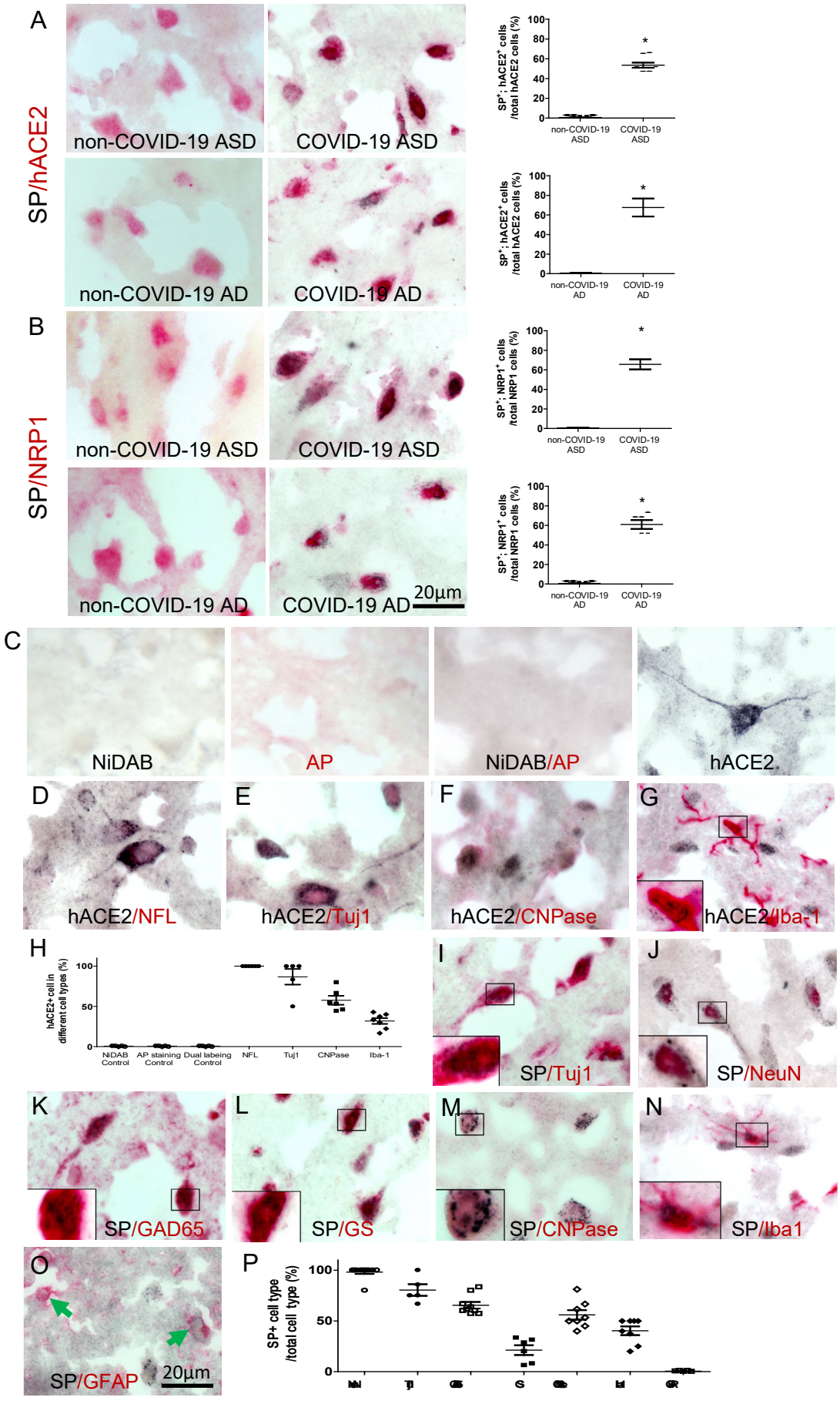
A
SP/hACE2
non-COVID-19 ASD
COVID-19 ASD
non-COVID-19 AD
COVID-19 AD
SP+; hACE2+ cells /total hACE2 cells (%)
B
SP/NRP1
SP+; NRP1+ cells /total NRP1 cells (%)
20µm
C
NiDAB
AP
NiDAB/AP
hACE2
D
hACE2/NFL
E
hACE2/Tuj1
F
hACE2/CNPase
G
hACE2/Iba-1
H
hACE2+ cell in different cell types (%)
NiDAB Control
AP staining Control
Dual labeing Control
NFL
Tuj1
CNPase
Iba-1
I
SP/Tuj1
J
SP/NeuN
K
SP/GAD65
L
SP/GS
M
SP/CNPase
N
SP/Iba1
O
SP/GFAP
20µm
P
SP+ cell type /total cell type (%)

Fig. 3

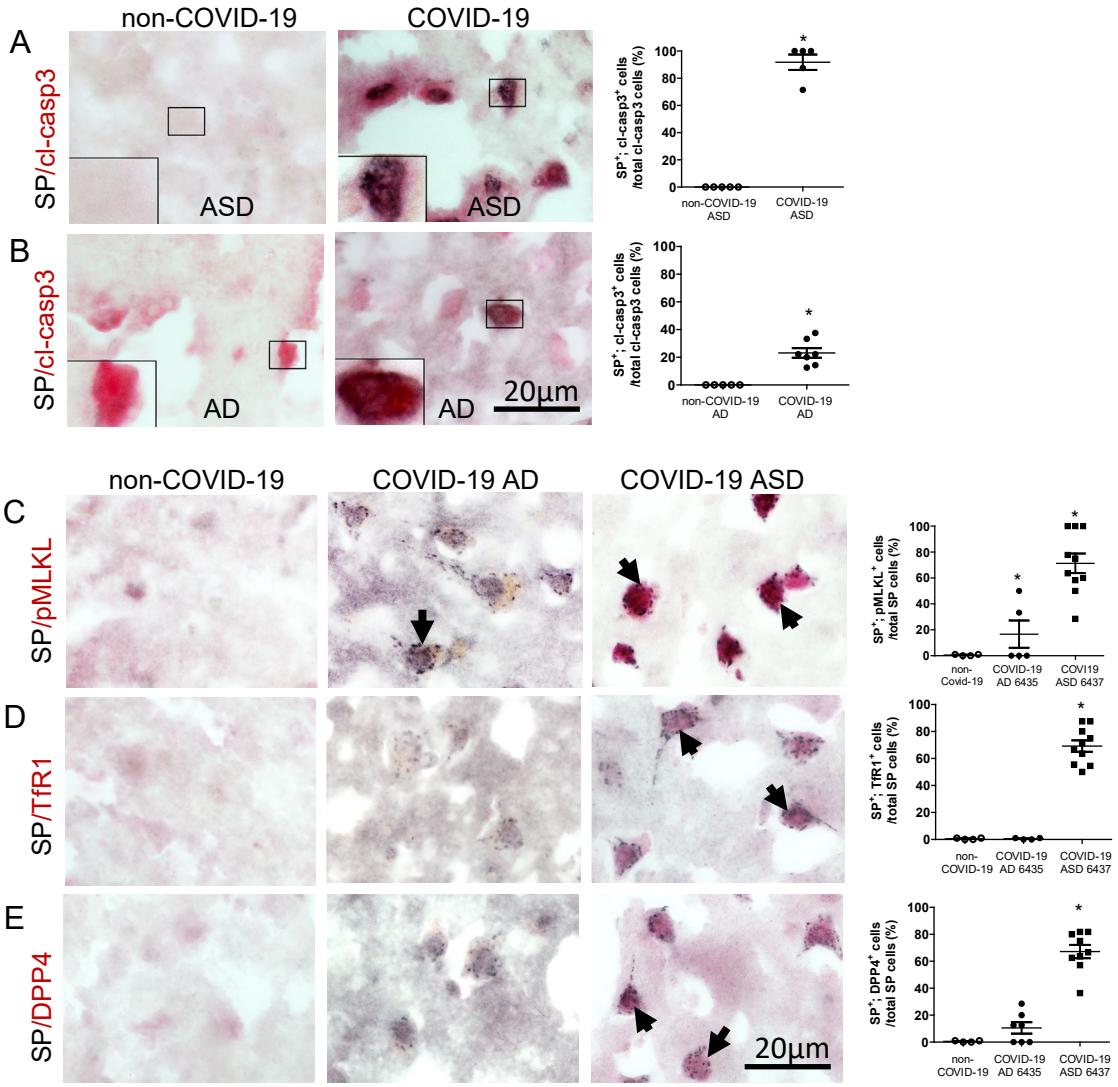
non-COVID-19
COVID-19
A
SP/cl-casp3
ASD
ASD
SP+; cl-casp3+ cells /total cl-casp3 cells (%)
non-COVID-19 ASD
COVID-19 ASD
B
SP/cl-casp3
AD
AD
20µm
non-COVID-19 AD
COVID-19 AD
non-COVID-19
COVID-19 AD 6435
COVI19 ASD 6437
C
SP/pMLKL
SP+; pMLKL+ cells /total SP cells (%)
D
SP/TfR1
SP+; TfR1+ cells /total SP cells (%)
COVID-19 ASD 6437
E
SP/DPP4
SP+; DPP4+ cells /total SP cells (%)
20µm

Fig. 4

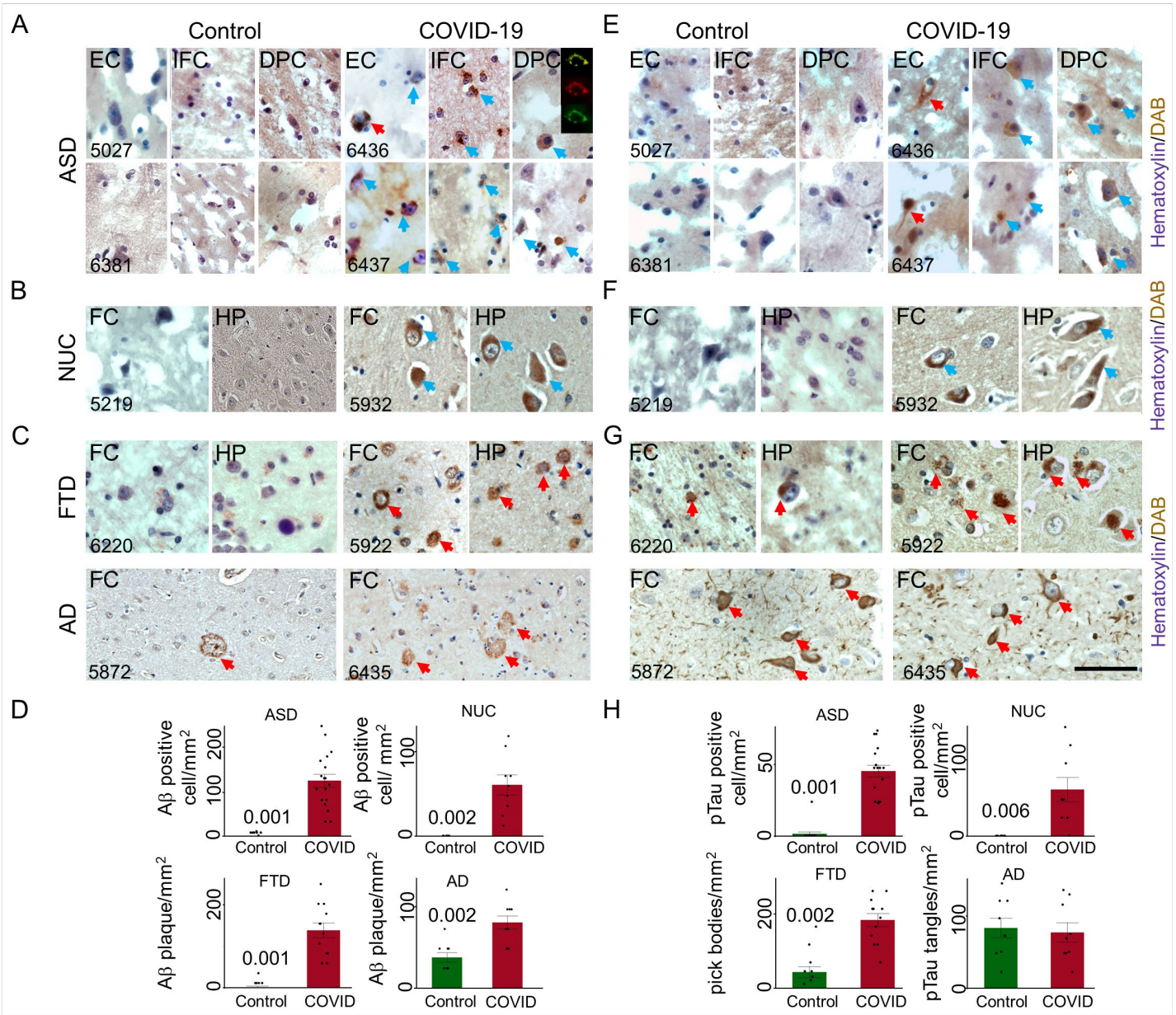
A
Control
COVID-19
EC
IFC
DPC
ASD
5027
6436
6381
6437
E
Hematoxylin/DAB
B
NUC
FC
HP
5219
5932
F
C
FTD
6220
5922
G
AD
5872
6435
D
Aβ positive cell/mm2
Aβ positive cell/ mm2
Aβ plaque/mm2
0.001
0.002
Control
COVID
H
pTau positive cell/mm2
pick bodies/mm2
pTau tangles/mm2
0.006

Fig. 5

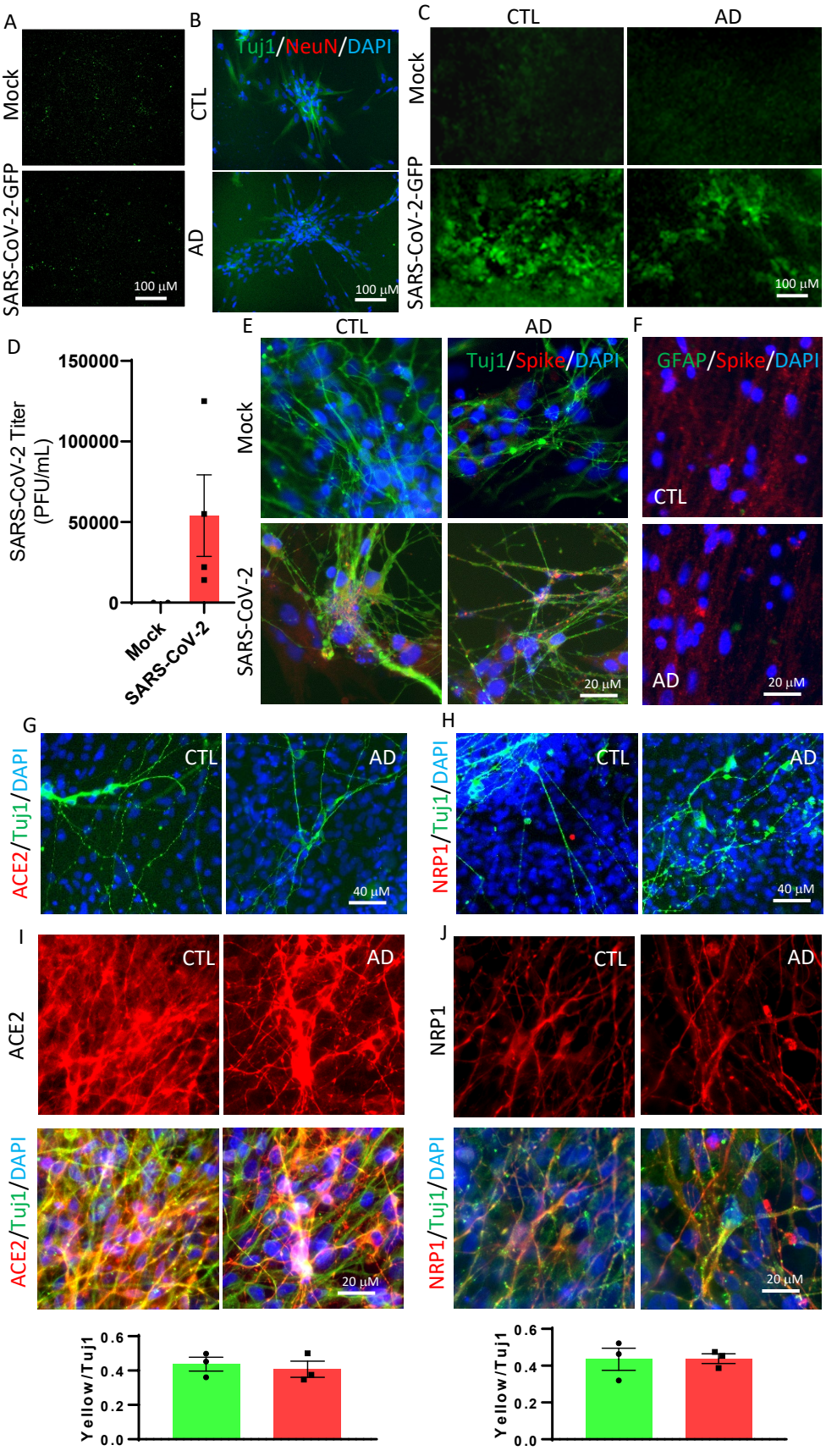
A
Mock
SARS-CoV-2-GFP
100 μM
B
Tuj1/NeuN/DAPI
CTL
AD
100 μM
C
CTL
AD
Mock
SARS-CoV-2-GFP
100 μM
D
SARS-CoV-2 Titer (PFU/mL)
150000
100000
50000
0
Mock
SARS-CoV-2
E
CTL
AD
Tuj1/Spike/DAPI
Mock
SARS-CoV-2
20 μM
F
GFAP/Spike/DAPI
CTL
AD
20 μM
G
ACE2/Tuj1/DAPI
CTL
AD
40 μM
H
NRP1/Tuj1/DAPI
CTL
AD
40 μM
I
ACE2
CTL
AD
ACE2/Tuj1/DAPI
20 μM
J
NRP1
CTL
AD
NRP1/Tuj1/DAPI
20 μM
Yellow/Tuj1
0.6
0.4
0.2
0.0
Yellow/Tuj1
0.6
0.4
0.2
0.0

Fig. 6

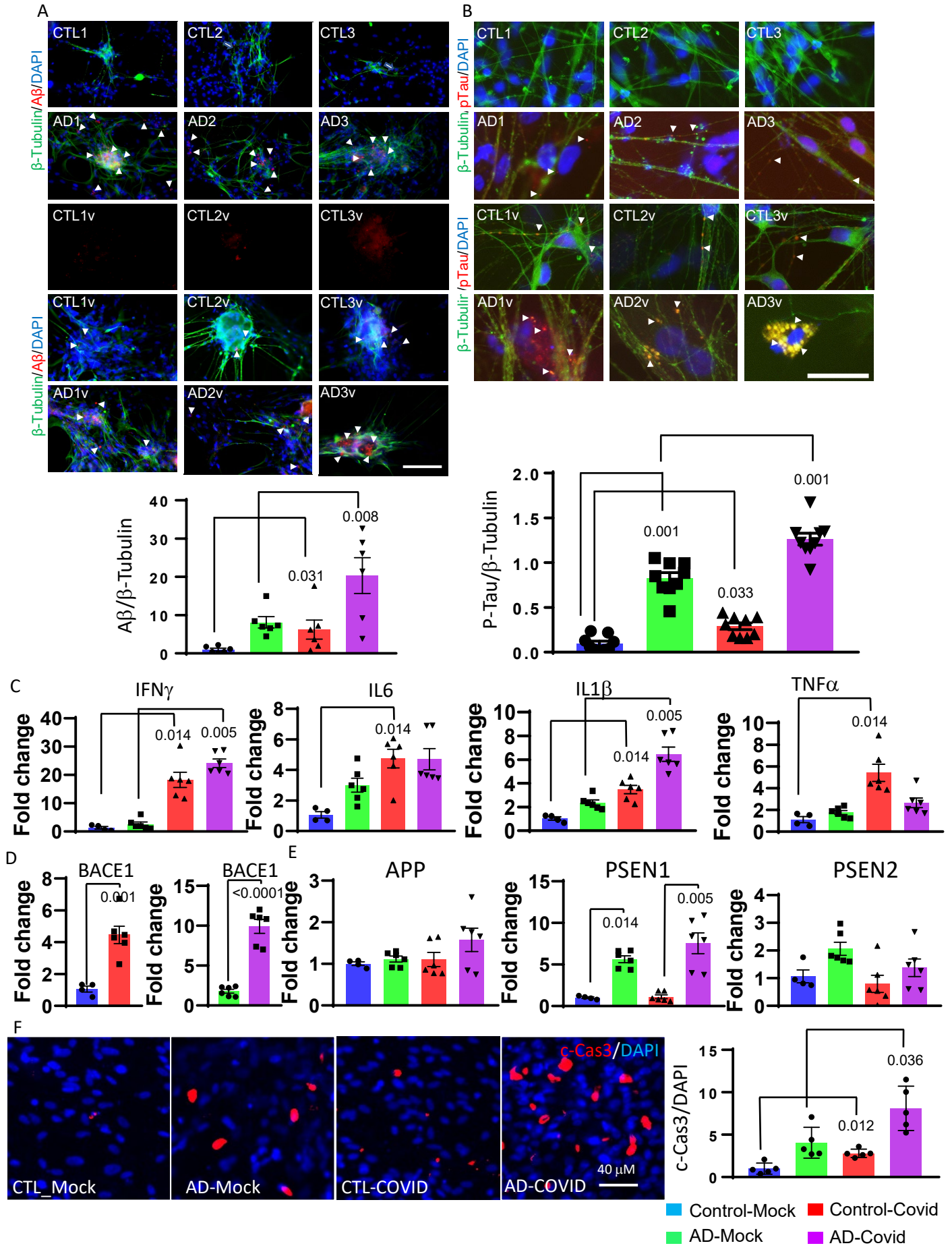
A
B
CTL1
CTL2
CTL3
AD1
AD2
AD3
CTL1v
CTL2v
CTL3v
AD1v
AD2v
AD3v
β-Tubulin/Aβ/DAPI
β-Tubulin, pTau/DAPI
Aβ/β-Tubulin
P-Tau/β-Tubulin
0.008
0.031
0.001
0.033
C
IFNγ
IL6
IL1β
TNFα
Fold change
0.014
0.005
D
BACE1
0.001
<0.0001
E
APP
PSEN1
PSEN2
F
c-Cas3/DAPI
CTL_Mock
AD-Mock
CTL-COVID
AD-COVID
40 μM
0.036
0.012
Control-Mock
Control-Covid
AD-Mock
AD-Covid

Fig. 7

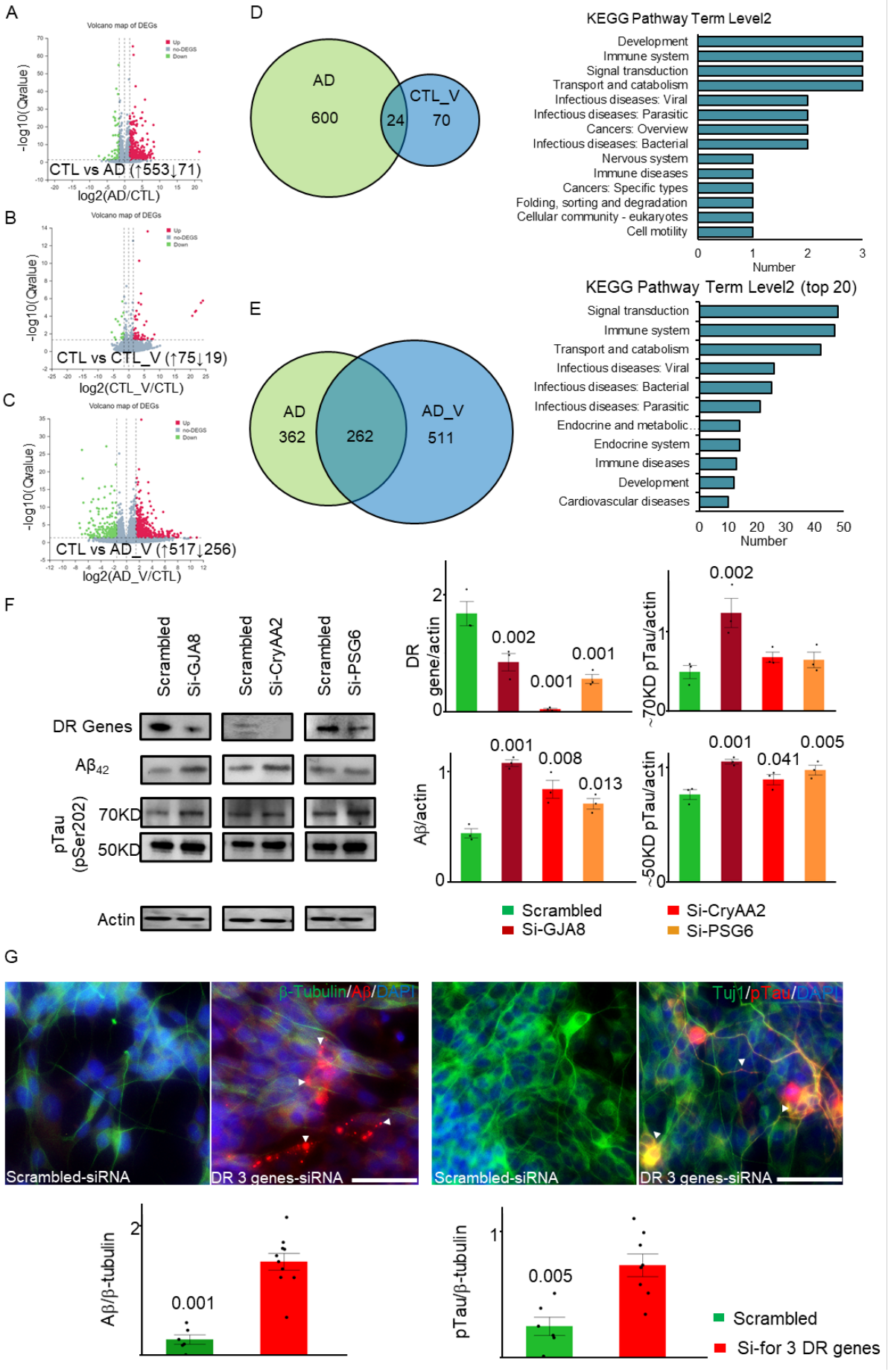
A
Volcano map of DEGs
-log10(Qvalue)
log2(AD/CTL)
CTL vs AD (↑553↓71)
B
Volcano map of DEGs
-log10(Qvalue)
log2(CTL_V/CTL)
CTL vs CTL_V (↑75↓19)
C
Volcano map of DEGs
-log10(Qvalue)
log2(AD_V/CTL)
CTL vs AD_V (↑517↓256)
D
AD
600
24
CTL_V
70
KEGG Pathway Term Level2
Development
Immune system
Signal transduction
Transport and catabolism
Infectious diseases: Viral
Infectious diseases: Parasitic
Cancers: Overview
Infectious diseases: Bacterial
Nervous system
Immune diseases
Cancers: Specific types
Folding, sorting and degradation
Cellular community - eukaryotes
Cell motility
Number
E
AD
362
262
AD_V
511
KEGG Pathway Term Level2 (top 20)
Signal transduction
Immune system
Transport and catabolism
Infectious diseases: Viral
Infectious diseases: Bacterial
Infectious diseases: Parasitic
Endocrine and metabolic..
Endocrine system
Immune diseases
Development
Cardiovascular diseases
Number
F
Scrambled
Si-GJA8
Scrambled
Si-CryAA2
Scrambled
Si-PSG6
DR Genes
Aβ42
pTau (pSer202)
70KD
50KD
Actin
DR gene/actin
0.002
0.001
0.001
~70KD pTau/actin
0.002
Aβ/actin
0.001
0.008
0.013
~50KD pTau/actin
0.001
0.041
0.005
Scrambled
Si-GJA8
Si-CryAA2
Si-PSG6
G
β-Tubulin/Aβ/DAPI
Scrambled-siRNA
DR 3 genes-siRNA
Tuj1/pTau/DAPI
Scrambled-siRNA
DR 3 genes-siRNA
Aβ/β-tubulin
0.001
pTau/β-tubulin
0.005
Scrambled
Si-for 3 DR genes

Methods

Mammalian iPSCs and culture conditions

Human iPSCs (1 cases of familial AD, 2 cases of sporadic AD, and 3 cases of apparently healthy controls) purchased from the Coriell Institute for Medical Research were used in our study. iPSCs were maintained on irradiated mouse CF-1 feeder layer (ATCC, Manassas, VA) at 37 ºC and 5% CO_2 in Knockout DMEM medium (Invitrogen, Waltham, MA) supplemented with 20% Knockout Serum Replacer (KSR) (Invitrogen, Waltham, MA), 0.1 mM nonessential amino acids (Invitrogen, Waltham, MA), 2 mM GlutaMAX (Invitrogen, Waltham, MA), 0.1 mM β-Mercaptoethanol (Sigma-Aldrich, St. Louis, MO), 10 ng/ml recombinant human basic fibroblast growth factor (Invitrogen, Waltham, MA) (hiPSC medium).

Viral strains

Vero E6 cells were maintained in EMEM (ATCC) media with 10% Serum Plus II Medium Supplement (Sigma-Aldrich). SARS-CoV-2 virus were obtained from the CDC following isolation from a patient in Washington State (WA-1 strain - BEI #NR-52281). SARS-CoV-2 GFP was generously provided by Dr. Ralph S. Baric. Stocks were prepared by infection of Vero E6 cells.

Brain Tissues

The major source for postmortem tissues is the Brain and Tissue Bank at University of Maryland (UMB). The Brain and Tissue Bank is a brain and tissue repository of the NIH NeuroBioBank. The Brain Tissue Bank is a national resource for investigators utilizing human post-mortem brain tissues and related biospecimens for research in understanding the conditions of the nervous system. All brain tissue is procured, stored, and distributed according to applicable State and

Federal guidelines and regulations involving consent, protection of human subjects and donor anonymity. All brain tissues we obtained from the Brain Tissue Bank are de-identified.

Following formalin-fixed brain tissues were obtained from the Brain and Tissue Bank at UMB: COVID-19 autism (ASD, ID #6436, 38 year-old, #6437, 30 year), COVID-19 Alzheimer's disease (AD, #6535, 77 year), age-matched non-COVID-19 controls (6 cases), non-COVID-19 ASD (6 cases), non-COVID-19 FTD (frontotemporal dementia, 4 cases), and apparently healthy subjects (9 cases). We also obtained 4 cases of non-COVID-19 AD from the NIH NeuroBioBank. Samples of three brain regions were obtained from individual: dorsolateral prefrontal cortex (Broca area 8), inferior frontal cortex (Broca area 44), entorhinal cortex.

Following frozen brain tissues were also obtained from the Brain and Tissue Bank. The frozen tissues were used for RNA extraction followed by reverse transcription and PCR detection of SARS-CoV-2 with CDC specific primers. The frozen tissues include SARS-CoV-2 infected lung and brain tissues (ASD, #6436), age-matched non-COVID-19 ASD controls and FTD controls.

In addition, paraffin sections and frozen brain tissues of the subjects of COVID-19 FTD (1 case) and COVID-19 individual without underlying condition, and non-COVID-19 AD (3 cases) were obtained from the Biomarker Laboratory and Biorepository at University of Southern California Alzheimer's Therapeutic Research Institute (USC ATRI) at University of California San Diego (UCSD).

Neuronal Cells

Primary Human Neurons were obtained from Neuromics (CA3 Bioscience, MN, USA). The cells were maintained in neuron growth medium supplemented (CA3 Bioscience, MN, USA) with 10% FBS at 37 °C in a humidified atmosphere of 5% CO_2 in culture flask.

Immunohistology staining of spike protein and markers of neural cells and programmed cell death

The formalin-fixed brain tissue blocks were immersed in 30% sucrose, then embed in OCT cryostat sectioning medium. The tissues were sectioned on a cryostat at 10 μm. After rehydrated, the sections were treated with 2% H_2O_2 for 15 minutes to quench the endogenous peroxidase. The staining was performed as previously described [1, 2]. Briefly, the slices were incubated with blocking solution consisting of 4% normal donkey serum (NDS), 0.2% triton (TX)-100 in phosphate-buffered saline (PBS) for 60 min, then with primary antibody diluted in blocking solution at 4 °C overnight. The slices were washed with PBS and incubated for 1 h in a biotinylated secondary antibody anti-mouse or rabbit (depending on the host species producing the primary antibodies). After three times of PBS washes, the sections were incubated in ABC solution (1:500; Vectastain Elite Kit) for 1h. The ABC solution was prepared and placed on ice for 30 minutes before use. Antibody labeling was then visualized via precipitation with a diaminobenzidine (DAB, 10mg/50ml) chromogen solution in PBS + 0.003% H_2O_2 (brown products) or with DAB in 0.175 M sodium acetate + 0.5% nickel ammonium sulfate + 0.003% H_2O_2 (for Ni-DAB staining, black products). If necessary, the sections were counterstained with hematoxylin before coverslip.

For immunohistology dual labeling, the sections were subject Ni-DAB staining with first primary antibody as described above. After PBS wash, the sections were re-blocked for 1 hours and following incubation with the second primary antibody at 4°C overnight. Next day, the sections were washed with PBS and incubated with alkaline phosphatase (AP)-conjugated goat secondary antibody (1:200) for 1 h, followed by incubation with AP red substrate (1:100) for 20-30 minutes.

DAB-stained sections were counterstained with hematoxylin. Sections were immersed in hematoxylin solution for 3 min and rinsed in running tap water until rinse water is colorless. After

differentiation by dipping slides 10 times in acid rinse solution (1% hydrochloric acid (HCl) in 70% ethanol), the slides were incubated in the bluing solution (1.5% lithium carbonate) for 30 s. There is no hematoxylin counterstaining performed for Ni-DAB or Ni-DAB/AP dual labeling before dehydrate and coverslip.

Dehydrate and coverslip sequence: 70% ethanol, 3 minutes; 95% ethanol I and II, 3 minutes for each; 100% ethanol I and II, 3 minutes for each; xylene I and II, 5 minutes for each. Mounting medium: Permount Mounting Medium.

Aβ and p-Tau Immunohistochemistry

β-amyloid (Aβ) and phospho-tau (pTau) Immunohistochemistry was carried out as previously described [3]. Briefly, the coronal sections were rehydrated, and endogenous peroxidase was quenched by treating with 0.3% H_2O_2. For Aβ staining, the antigen retrieval was carried by using 70% formic acid for 20 minutes. Antigen retrieval for the other antibodies was by autoclaving at 120°C for 5 min. The primary antibody was applied on the sections at 4°C overnight, followed by 60-min incubation with specific secondary antibody coupled with HRP (Histofine simple stain MaxPo M/R, Nichirei Bioscience Inc., Japan) at room temperature. DAB reaction was performed to visualize the color. All antibody dilutions and washing steps were performed in phosphate buffer, pH 7.2. HRP intensities and cell counts in 3 different regions (Frontal Cortex, Entorhinal Cortex) in three sections/slices from each group were measured using the ImageJ Fiji platform. Data were represented as staining intensity per square millimeter. Because the MaxPo M/R antibodies are Fab fragments, the blocking is not necessary.

Thioflavin staining

The Aβ staining Thioflavin-T were performed following the similar antigen protocol. After blocking with 5% goat serum for 30 minutes overnight incubation with anti Aβ antibody 6E10

were performed. In the following day the brain sections were probed with Alexa-fluor594 labeled secondary antibody. After an extensive washing, Thioflavin-T (0.1% in 50% DMSO) were applied over the brain sections for 5 minutes. An extensive washing was performed using PBS containing 0.05% tween20. Furthermore, the fluorescent background was quenched with Tureblack (Biotium, USA). Thioflavin-T and Alexa-fluor594 intensity were measured using a fluorescence laser microscope (LSM780, Zeiss, Germany).

Immunofluorescence staining

For immunofluorescence staining, cells were cultured on a collagen-coated coverslip. After specific treatments, cells were fixed with 4% paraformaldehyde-PBS. The cell membrane was permeabilized with 0.25% Triton-X100 and/or 5 mg/ml digitonin followed by blocking with 5% BSA. After probing with primary antibodies, specific Alexa-fluor labeled secondary antibody were used. 4',6-Diamidino-2-phenylindole dihydrochloride (DAPI) staining was used to visualize the nuclei (Thermo Fisher Scientific). Fluorescence was assessed using a fluorescence laser microscope (LSM780, Zeiss, Germany).

Detection of SARS-CoV-2 RNA using RNAscope

RNA *In situ* hybridization in FFPE slides was performed by using the RNAScope 2.5 HD Detection (RED) Kit (ACD, CA), based on the protocol provided by the manufacturer. Briefly, after deparaffinization and antigen retrieval, the slides were hybridized with the 40-ZZ positive-sense RNA probe, V-SARS-CoV-2-S (Ref#: 854841, ACD) in the oven at 40 ºC for 2 hours. We then washed the slides with 1 X Wash Buffer for 2 min twice. The remaining hybridization procedure at 40 ºC include: 1) Amp 1, 30 min; 2) Amp 2, 15 min; 3) Amp, 30 min; 4) Amp 4, 15 min; 5) Amp 5, 30 min, and 6) Amp 6, 15 min with an interval of repeated 1X Wash buffer for 2 min. Subsequently, the signals were detected by incubating with a mixture of RED-B and RED-A

at ratio of 1:60 for 10 min at room temperature followed by counterstaining with 50% hematoxylin for 2 min.

Generation of human induced pluripotent stem cells (hiPSCs)

Human fibroblast from Coriell Institute were induced into pluripotent stem cell with CMV promoter Thomson factors lentivirus set which contains Lenti-virus harboring Oct4, Sox2, Nanog, and Lin28 (Cat#: G353, ABM Inc., Canada). Briefly, human fibroblasts were seeded on 6 well plate with 8 x 10^4 per well at day -2 and transduced with Lenti-virus particles (MOI of 4:3:3:3). Cells were cultured for 7 days and replated at 2 x 10^4 cells per well of 6 well plate on irradiated mouse embryonic fibroblasts (MEF) feeder layer. From day 8, medium was replaced with Knockout DMEM (Invitrogen) supplemented with 20% Knockout Serum Replacer (KSR, Invitrogen), 0.1 mM nonessential amino acids (Invitrogen), 2 mM GlutaMAX (Invitrogen), 0.1 mM β-mercaptoethanol (Sigma-Aldrich, St. Louis, MO), 10 ng/ml recombinant human basic fibroblast growth factor (Invitrogen) (hiPSC medium). On week 3-4, iPSCs were identified from morphology change and picked out into 48-well plates with MEF feeder.

Neuron differentiation from hiPSCs.

hiPSCs were differentiated into neurons as described with modification (Nat Med. 2018 May;24(5):647-657). hiPSCs dissociated with collagenase IV (Stem Cell Technologies) were cultured in suspension to form embryoid bodies (EB) in hES medium without bFGF for 5 days followed by maintenance in NIM medium containing Dulbecco's modified Eagle's medium/F12 and Neurobasal Medium (1:1, Thermo Fisher), 1% N2 Supplement (Life Technologies), 1% B27 Supplement (Life Technologies), nonessential amino acids, and 0.5% penicillin/streptomycin (Life Technologies) supplemented with inhibitors of the TGF-β receptor (SB431542, Stemgent; 5 μM) and the bone morphogenetic protein receptor (LDN-193189, Stemgent; 0.25 μM). On day 7,

spheres were transferred to wells coated with Matrigel (BD Biosciences) and grown in NPM medium which is same to NIM medium but replace SB431542 and LDN-193189 with 10 ng/ml bFGF (PeproTech), 10 ng/mL epidermal growth factor (EGF) (PeproTech), and 2 μg/ml heparin (Sigma). On day 15, medium was changed to NDM medium which is same to NPM medium but replace bFGF, EGF and heparin in NPM with brain-derived neurotrophic factor (10 ng/ml; PeproTech), and glial cell–derived growth factor (10 ng/ml; PeproTech). Around day 20, neurons were observed and were further differentiated for 30 days.

Immunofluorescence staining in iPSCs-derived neurons

Neurons derived from AD or Control (from healthy individuals) hiPSCs with or without SARS-CoV-2 infection were fixed in 4% paraformaldehyde (PFA) for 10 minutes followed by blocking in 5% bovine serum albumin in PBST (0.1% Triton X-100 in PBS) for 10 minutes. The following antibodies were used as primary antibodies: Spike (1:200), Tuj1 (1:500), ACE2 (1:200), NRP1 (1:200), NeuN (1:200), GFAP (1:200), c-Cas3 (1:200). Normal rabbit or mouse IgG using the same dilutions as primary antibodies were used as controls. After washing with PBS, neurons were incubated with secondary antibodies. Then, neurons were counterstained with DAPI and mounted with aqueous mounting medium (Sigma, St Louis, MO). Images were captured under a microscope (Keyence BZ X700, Osaka, Japan).

SARS-CoV-2 production and infection of hiPSCs derived neurons

The stock of SARS-CoV-2 virus (CDC, WA-1 strain - BEI #NR-52281, and SARS-CoV-2 GFP generously provided by Dr. Ralph S. Baric, at the Department of Epidemiology and Department of Microbiology and Immunology, University of North Carolina at Chapel Hill), were prepared by infection of Vero E6 cells for two days when CPE (cytopathic effects) was starting to become visible. Media were collected and clarified by centrifugation prior to being aliquoted for storage

at −80 °C. Neurons derived from hiPSCs were infected with SARS-CoV-2 at 5 x 10^3, 1 x 10^4, or 2 x 10^4 plaque forming units (pfu) per well of 6 well plate for 48 h in NDM medium. All work with infectious virus was performed in a Biosafety Level 3 laboratory and approved by our Institutional Biosafety Committee.

SARS-CoV-2 Titering by semi-solid plaque assay

VeroE6 cells were plated in 12 well plates with 2x10^5 cells per well one day prior to processing. On the day of processing, samples were serially diluted 1:10 and 200uL of each sample dilution was added to each well in singlet and incubated for 1 hour at 37°C (5% CO2) with rocking every 15 minutes. Following incubation, 2 mL of a semi-solid agar overlay, DMEM (gibco) containing 4% fetal bovine sera (gibco) and 2% agarose, was added to each well. Plates are incubated for 3 days at 37°C (5% CO2) before plates were fixed with 4% paraformaldehyde, stained with crystal violet stain, and plaques counted.

Neural maturation, siRNA Transfection, and Lenti virus transduction

Primary Human Neurons obtained from Neuromics (Edina, MN) grow for four weeks in the Neuromics growth medium supplemented with brain derived neurotropic factor (BDNF). Medium were changed every 2 days. For further experiment, cells were plated on a 6-well plate in neuron growth medium supplemented with 5% FBS. siRNA transfection was carried out using X-tremeGENE siRNA transfection reagent (Roche, Basel, Switzerland) at 60% cell confluency. Medium was replaced with fresh medium 24 hours post-transfection and maintained for additional 48 hours. Lentivirus mediated overexpression of the FCGR, LILRB5 and OTOR carried out using virus particles obtained from OriGene (Rockville, MD). Virus transduction were carried out at 5.0 MOI using polybrene. GFP expressing lenti-particles were used as the control.

RNA sequencing

mRNAs were extracted from neurons derived from AD or Control hiPSCs with or without SARS-CoV-2 infection and sequenced at BGI on DNBSeq platform. Briefly, mRNAs were extracted with Trizol reagent. First-strand cDNA was generated using random hexamer-primed reverse transcription, followed by a second-strand cDNA synthesis. The synthesized cDNA was subjected to end-repair and then was 3' adenylated. Adapters were ligated to the ends of these 3' adenylated cDNA fragments, followed by PCR. PCR products were purified with Ampure XP Beads and dissolved in EB solution. Library was validated on the Agilent Technologies 2100 bioanalyzer. The double stranded PCR products were heat denatured and circularized by the splint oligo sequence. The single strand circle DNA were formatted as the final library. The library was amplified with phi29 to make DNA nanoball (DNB) which had more than 300 copies of one molecular. The DNBs were load into the patterned nanoarray and single end 50 (pair end 100) bases reads were generated in the way of sequenced by synthesis.

Quantitative reverse transcription PCR

mRNAs were extracted from neurons derived from AD or Control hiPSCs with or without SARS-CoV-2 infection in Trizol reagent (Thermofisher, Waltham, MA) and followed by cDNA synthesis with SuperScript™ III Reverse Transcriptase kit (ThermoFisher). RT-PCR were performed with PowerUp™ SYBR™ Green Master Mix (ThermoFisher) with 45 cycles and PCR products were loaded into 2% agarose gel and run at 75 v for 5.5 h. Gel Image were recorded with Bio-Rad ChemiDoc MP imaging system (Hercules, CA).

QUANTIFICATION AND STATISTICAL ANALYSIS

In the experiment assessing the impact of SARS-CoV-2 virus on the brain pathology, we analyzed (a) 5 Covid19 samples consisting of AD-Covid19 (1 case), FTD-Covid19 (1 case), ASD-Covid19

(2 cases), and Covid-19 without underlying condition (1 case); (b) 6 cases of sporadic AD as the controls; and (c) 8 cases of age-matched, non-Covid-19 healthy controls. Labeled cells from at least 3 random fields ($n \geq 3$) were counted. Data are presented as the means ± standard errors (SEs). Student's t test was used for two group comparisons. One-way ANOVA was performed for comparisons of more than two group using graphPad prism software v7. In ANOVA, a *Tukey* test was used to estimate the significance between groups. Differences were considered statistically significant when $P < 0.05$.

In the experiment with cell culture studies, we differentiated neurons from 3 iPSC lines derived from AD fibroblast cells and 3 lines from healthy subjects as the controls. The experiments were repeated in triplicate as we previously described [4, 5]. Data are presented as the means ± standard errors (SEs). Student's *t* test was used for two group comparisons. One-way ANOVA plus *Tukey* test was performed for comparisons of more than two group. Differences were considered statistically significant when $P < 0.05$.

Reference:

[1] Shen WB, McDowell KA, Siebert AA, Clark SM, Dugger NV, Valentino KM, et al. Environmental neurotoxin-induced progressive model of parkinsonism in rats. Ann Neurol. 2010;68:70-80.
[2] Shen WB, Plachez C, Tsymbalyuk O, Tsymbalyuk N, Xu S, Smith AM, et al. Cell-Based Therapy in TBI: Magnetic Retention of Neural Stem Cells In Vivo. Cell Transplant. 2016;25:1085-99.
[3] Elahi M, Hasan Z, Motoi Y, Matsumoto SE, Ishiguro K, Hattori N. Region-Specific Vulnerability to Oxidative Stress, Neuroinflammation, and Tau Hyperphosphorylation in Experimental Diabetes Mellitus Mice. J Alzheimers Dis. 2016;51:1209-24.
[4] Xu C, Shen W-B, Reece EA, Hasuwa H, Harman C, Kaushal S, et al. Maternal diabetes induces senescence and neural tube defects sensitive to the senomorphic rapamycin. Science Advances. 2021;7:eabf5089.
[5] Wang F, Wu Y, Gu H, Reece EA, Fang S, Gabbay-Benziv R, et al. Ask1 gene deletion blocks maternal diabetes-induced endoplasmic reticulum stress in the developing embryo by disrupting the unfolded protein response signalosome. Diabetes. 2015;64:973-88.

Table S1. Relative numbers of spike protein$^+$ cells in 5 COVID-19 cases

ID#	Disease	Age	EC	DPC	IFC
6435	COVID-19, AD	77	++	++	++
6436	COVID-19, ASD	38	++	++	++
6437	COVID-19, ASD	30	++	++	+++
5932	COVID-19, NUC	71	Not tested	Not tested	+
5922	COVID-19, FTD	70	Not tested	Not tested	+

AD: Alzheimer's disease; ASD: autism; EC: entorhinal cortex; DPC: dorsolateral prefrontal cortex; IFC: inferior frontal cortex. FTD: frontotemporal dementia. NUC: no underlying condition. +++: >200 spike protein$^+$ cells/mm^2; ++: 100-200 spike protein$^+$ cells/mm^2; +: <100 spike protein$^+$ cells/mm^2

Fig. S1

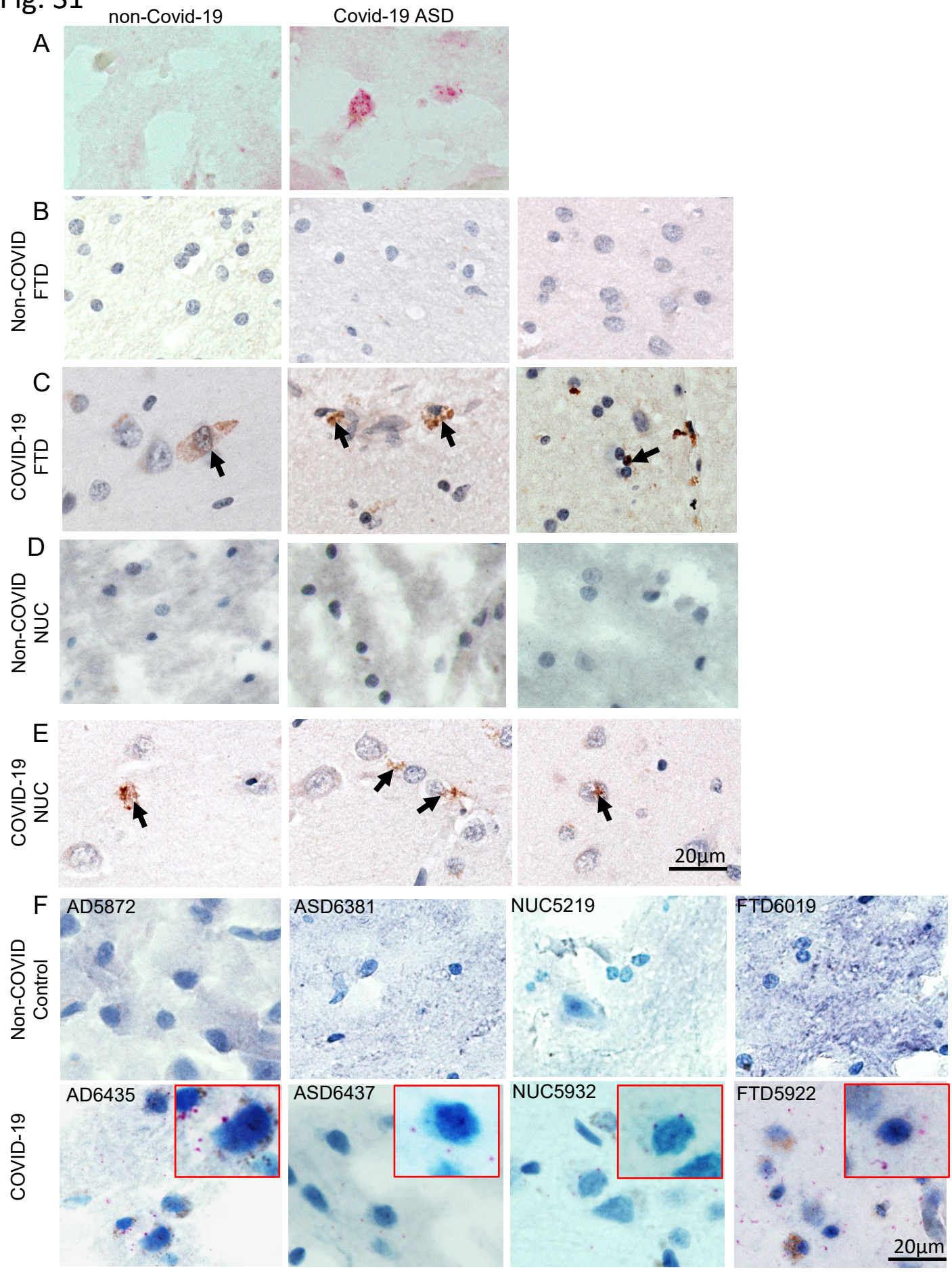
non-Covid-19
Covid-19 ASD
A
B
Non-COVID
FTD
C
COVID-19
FTD
D
Non-COVID
NUC
E
COVID-19
NUC
20µm
F
Non-COVID
Control
AD5872
ASD6381
NUC5219
FTD6019
COVID-19
AD6435
ASD6437
NUC5932
FTD5922
20µm

Fig. S2

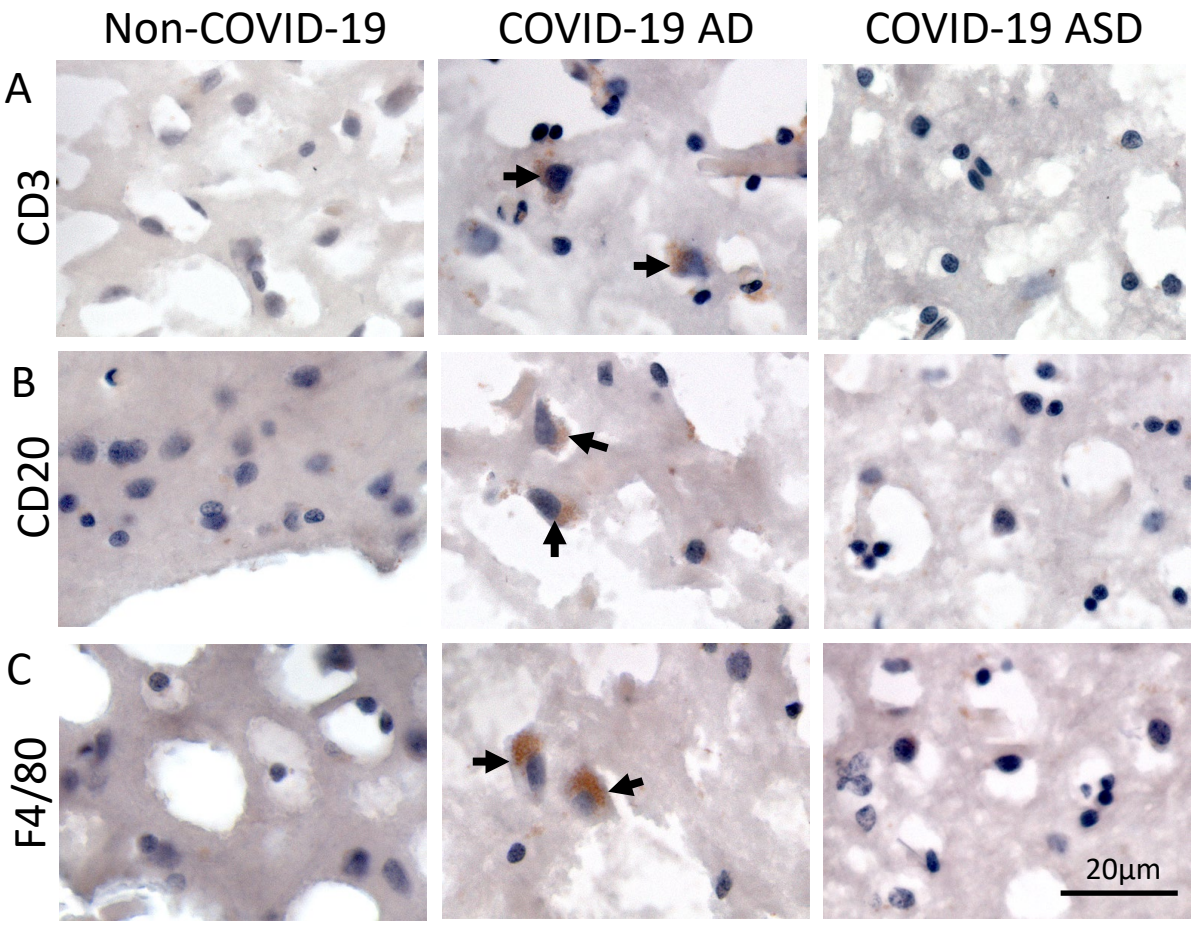
Non-COVID-19
COVID-19 AD
COVID-19 ASD
A
CD3
B
CD20
C
F4/80
20μm
D
CD3
CD20
F4/80
immune cells (%)
40
30
20
10
0
*
COVID-19
-
+
+
Control
AD
ASD

Fig. S3

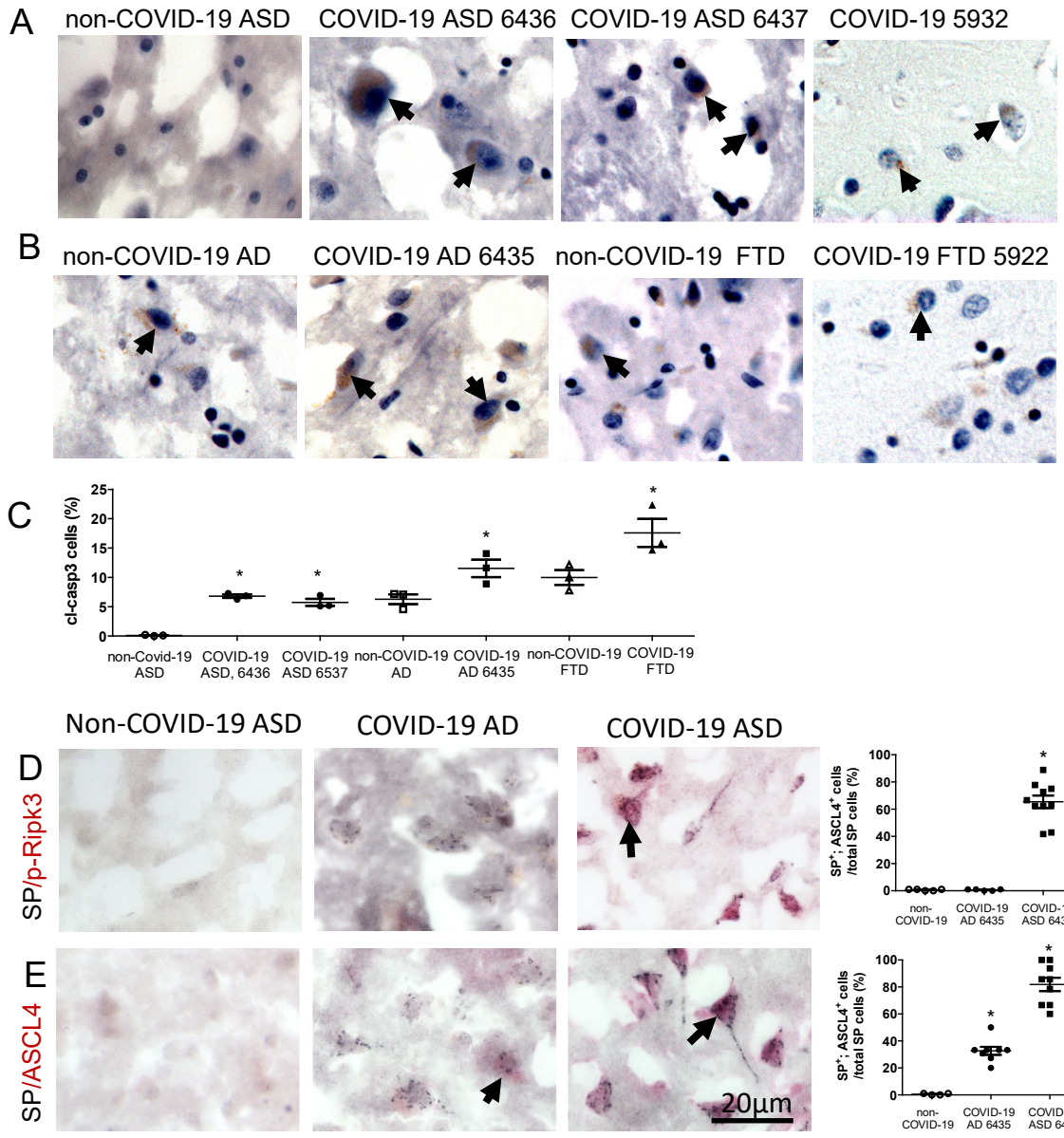
A
non-COVID-19 ASD
COVID-19 ASD 6436
COVID-19 ASD 6437
COVID-19 5932
B
non-COVID-19 AD
COVID-19 AD 6435
non-COVID-19 FTD
COVID-19 FTD 5922
C
cl-casp3 cells (%)
25
20
15
10
5
0
non-Covid-19 ASD
COVID-19 ASD, 6436
COVID-19 ASD 6537
non-COVID-19 AD
COVID-19 AD 6435
non-COVID-19 FTD
COVID-19 FTD
Non-COVID-19 ASD
COVID-19 AD
COVID-19 ASD
D
SP/p-Ripk3
SP+; ASCL4+ cells /total SP cells (%)
100
80
60
40
20
0
non-COVID-19
COVID-19 AD 6435
COVID-19 ASD 6437
E
SP/ASCL4
SP+; ASCL4+ cells /total SP cells (%)
100
80
60
40
20
0
non-COVID-19
COVID-19 AD 6435
COVID-19 ASD 6437
20µm

Fig. S4

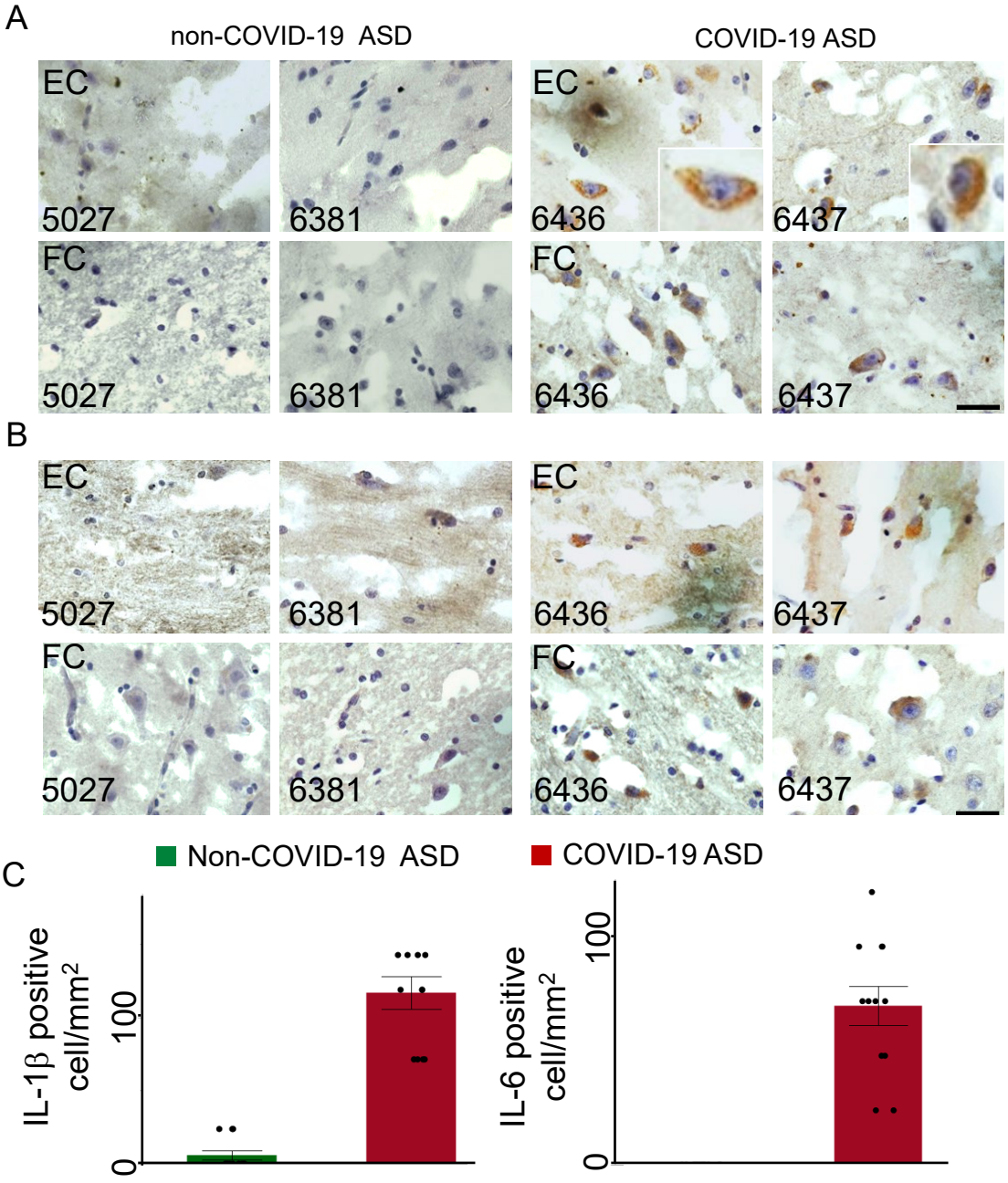
A
non-COVID-19 ASD
COVID-19 ASD
EC
FC
5027
6381
6436
6437
B
C
Non-COVID-19 ASD
COVID-19 ASD
IL-1β positive cell/mm²
IL-6 positive cell/mm²
100
0

Fig. S5

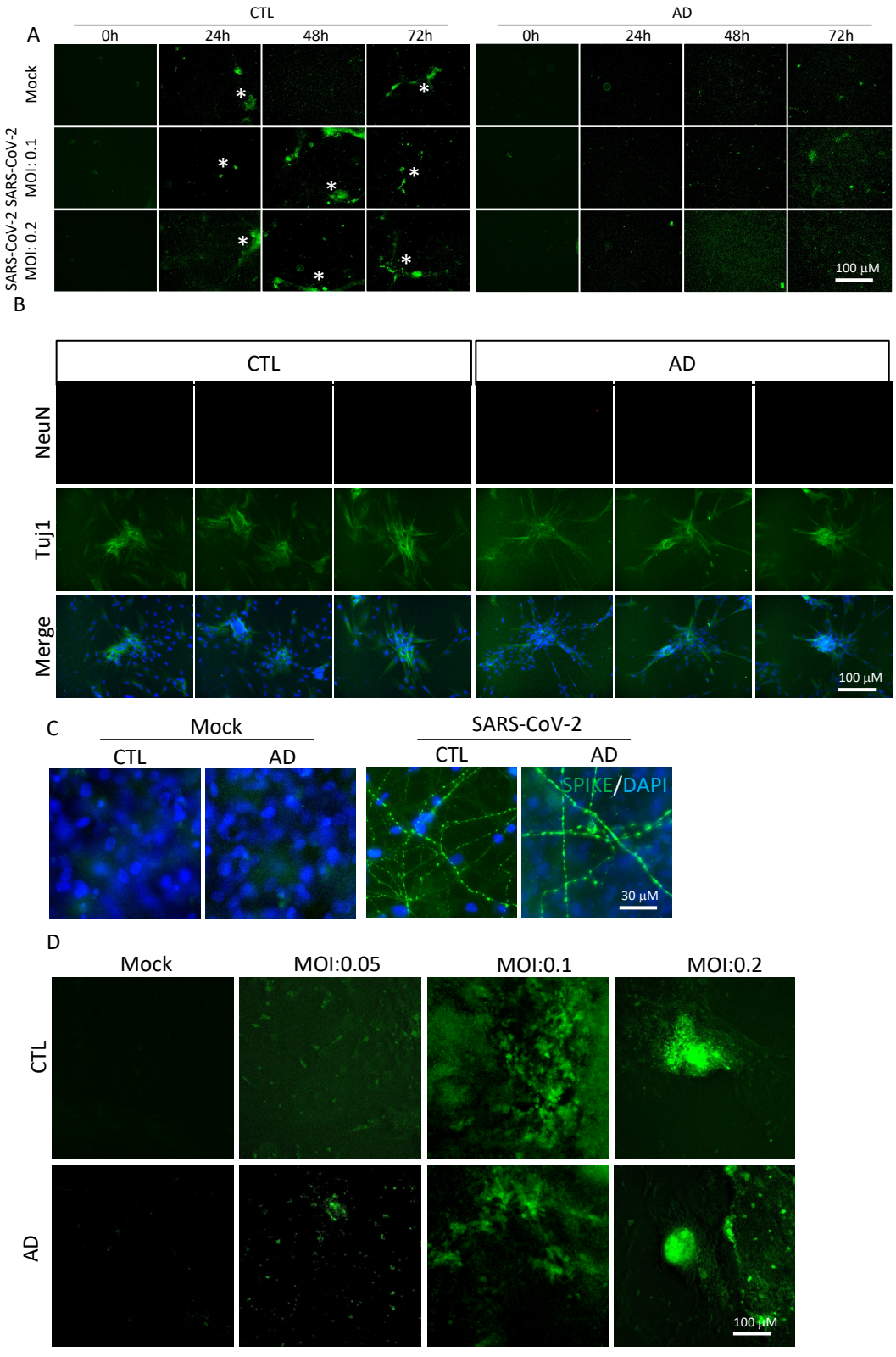
A
CTL
AD
0h
24h
48h
72h
Mock
SARS-CoV-2 MOI: 0.1
SARS-CoV-2 MOI: 0.2
100 μM
B
CTL
AD
NeuN
Tuj1
Merge
100 μM
C
Mock
SARS-CoV-2
CTL
AD
SPIKE/DAPI
30 μM
D
Mock
MOI:0.05
MOI:0.1
MOI:0.2
CTL
AD
100 μM

Fig. S6

A

Gene	CTL/AD	CTL/AD_V
XAF1	1.60	3.58
TWIST2	1.81	3.96
CASP4	1.55	3.17
CD34	1.82	3.54
CCL4	2.83	5.49
CCL3	3.40	6.44
KLHDC7B	1.79	3.33
LILRB1	4.37	8.12
GJB2	1.84	3.40
LAIR1	1.92	3.38
PLA2G7	2.08	3.66
C3	2.31	4.05
FIBIN	1.67	2.85
HCK	1.99	3.36
SP140L	1.60	2.68
COMP	1.69	2.83
SLC22A4	1.53	2.53
LRRC25	2.42	3.91
CTSS	2.38	3.78
SLAMF8	2.16	3.36
FERMT3	3.28	5.09
NPL	1.55	2.38
ITGAL	2.83	4.32
AOAH	2.29	3.48
CCL3L1	5.34	8.10

Deteriorated fold > 1.5
Upregulated genes

B

Gene	CTL/AD	CTL/AD_V
PLA2G2F	-1.58	-5.46
CRYAA2	-1.88	-5.82
ABCB11	-1.65	-4.64
GJA8	-1.81	-5.06
CRYBB3	-1.76	-4.11
CRYBB1	-2.58	-5.90
C1orf105	-1.65	-3.70
CRYBA1	-2.68	-6.02
MIP	-3.11	-6.95
CRYBA4	-2.58	-5.66
GPD1	-1.60	-3.43
BHMT	-2.52	-5.31
PITX3	-2.07	-4.33
CRYBA2	-3.24	-6.72
GJA3	-1.63	-3.38
CRYGS	-2.73	-5.65
PSG7	-3.39	-6.95
PSG3	-3.17	-6.45
KMO	-1.78	-3.62
PSG2	-3.57	-7.24
CRYGD	-1.83	-3.70
CRYAB	-2.33	-4.53
CRYBB2	-2.84	-5.46
HSD3B1	-1.60	-2.96
PROX1	-1.67	-2.99
VIT	-1.68	-2.99
ERICH5	-1.59	-2.80
AQP5	-1.70	-2.96
PSG1	-2.66	-4.61
COLGALT2	-1.56	-2.61
CRYGC	-2.69	-4.45
ANKRD34C	-2.56	-4.18
DBX2	-2.75	-4.29
MAMDC2	-1.68	-2.54

C

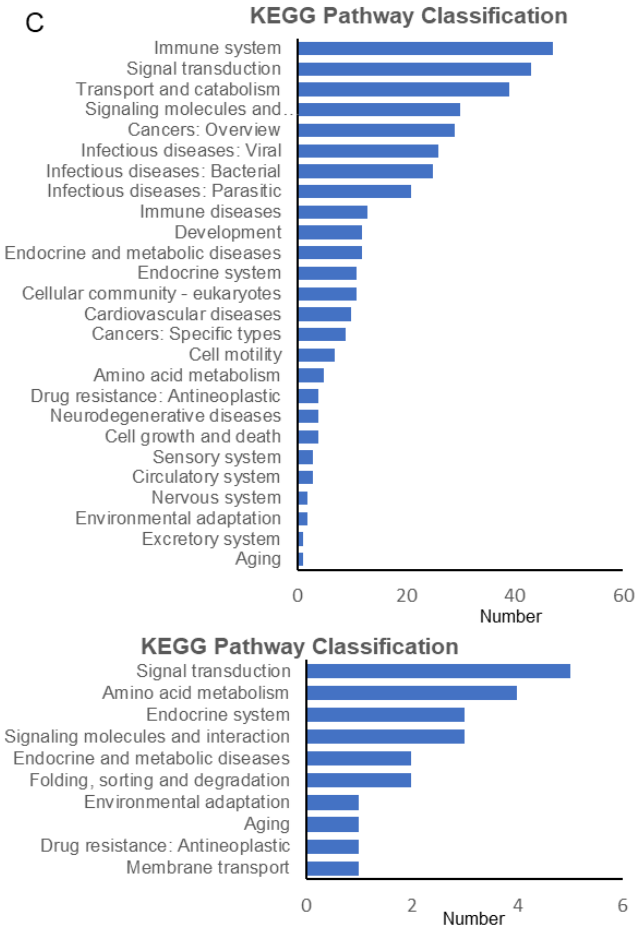

D

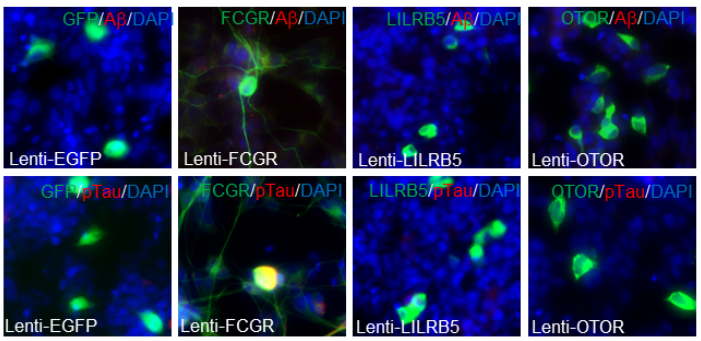

E

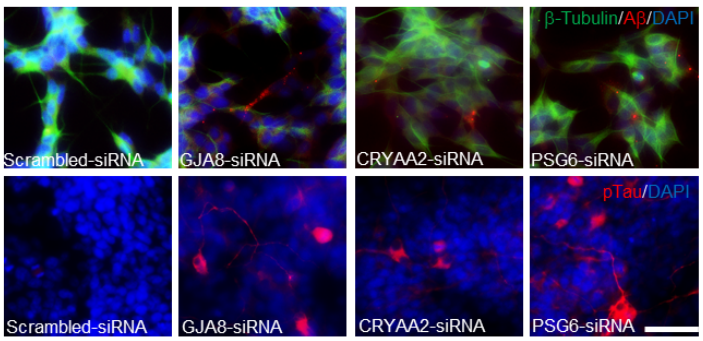

Resource Tables

Antibody	Sources	Identifier
Rabbit anti-SARS-CoV-2 spike glycoprotein antibody	Abcam	Cat# ab272504; RRID: AB_2847845
Rabbit anti-SARS Nucleocapsid Protein Antibody	Novus	Cat# NB100-56576; RRID:AB_838838
Rabbit anti-human ACE2 polyclonal antibody	Thermo Fisher Scientific	Cat# PA5-20046; RRID: AB_1115262
rabbit anti-neuropilin-1 antibody	Abcam	Cat# ab81321; RRID: AB_164073
Mouse anti-Glutamate Decarboxylase, 65 kDa Isoform (GAD65), clone GAD-6 antibody	millipore	Cat# mAB351; RRID: AB_2263126
Mouse anti-Glutamine Synthetase, clone GS-6 antibody	millipore	Cat# MAB302; RRID: AB_2110656
Rabbit anti-NeuN antibody	Abcam	Cat# ab177487; RRID: AB_2532109
Anti-Galactocerebroside antibody produced in rabbit	Sigma-Aldrich	Cat# 9152; RRID: AB_259984
Rabbit anti-Glial Fibrillary Acidic Protein (GFAP) antibody	Agilent	Cat# Z0334; RRID: AB_10013382
Anti-β-Amyloid, 1-16 Antibody (Previously Covance catalog# SIG-39300)	Biolegend	Cat# 803014; RRID:AB_2728527
β-Amyloid (D3D2N) Mouse mAb	Cell Signaling Technology	Cat# 15126; RRID:AB_2798720
Rabbit anti-phospho-Tau (Ser202, Thr205) Monoclonal Antibody (AT8)	Thermo Fisher Scientific	Cat# MN1020; RRID: AB_223647
Anti-β-Amyloid (D54D2) XP® Rabbit mAb antibody	Cell Signaling Technology	Cat# 8243; RRID: AB_2797642
Neurofilament-L (C28E10) Rabbit mAb antibody	Cell Signaling Technology	Cat# 2837; RRID: AB_823575
Rabbit anti-Cleaved Caspase-3 (Asp175) Antibody	Cell Signaling Technology	Cat# 9661; RRID: AB_2341188
Neuronal Class III beta-Tubulin (TUJ1) Mouse Monoclonal Antibody, Purified	Covance	Cat# MMS-435P; RRID: AB_231377
Rabbit anti Iba1, Rabbit antibody	FUJIFILM Wako	Cat# 019-19741; RRID:AB_839504
Rabbit anti-RIP3 (phospho S227) antibody [EPR9627]	Abcam	Cat# ab209384; RRID: AB_2714035
Rabbit anti-MLKL (phospho S358) antibody	Abcam	Cat# ab187091; RRID: AB_2619685
Mouse anti-TRANSFERRIN RECEPTOR Monoclonal Antibody (H68.4)	Thermo Fisher Scientific	Cat# 13-6800; RRID: AB_86623

Rabbit anti-FACL4 (ASCL4) antibody [EPR8640]	Abcam	Cat# ab155282; RRID: AB_2714020
Rabbit anti-DPP4/CD26 (D6D8K) antibody	Cell Signaling Tech	Cat# 67138; RRID: AB_2728750
Rabbit anti-phospho-Tau (Ser396) Polyclonal Antibody	Thermo Fisher Scientific	Cat# 44-752G; RRID: AB_253374
Rabbit anti-phospho-Tau (Ser214) Polyclonal Antibody	Thermo Fisher Scientific	Cat# 44-742G; RRID: AB_2533740
Rabbit anti-pTau-Ser202(PS202) antibody	In house	
Rabbit Anti-Amyloid oligomer, abeta, oligomeric antibody	Millipore	Cat# AB9234; RRID: AB_570955
Human IL-1 beta/IL-1F2 MAb (Clone 8516) antibody	R and D System	Cat# MAB201; RRID:AB_358006
Mouse Anti-Human IL-6 Monoclonal antibody, Unconjugated, Clone 1936	R and D System	Cat# MAB2061; RRID: AB_2127616
CD3 Monoclonal Antibody (OKT3), Functional Grade	Thermo Fisher Scientific	Cat# 16-0037-81; RRID: AB_468854
Mouse anti-human CD20 antibody	Biolegend	Cat# 302301; RRID:AB_314249
F8/40 mouse monoclonal antibody	Santa Cru Biotech	Cat# sc377009
Biotin-conjugated Goat anti-mouse IgG	Vector Lab	Cat# BA-9200; RRID:AB_2336171
Biotin-conjugated Goat anti-Rabbit IgG	Vector Lab	Cat# BA-1000; RRID:AB_2313606
Alexa488-donkey anti-mouse IgG	Invitrogen	Cat# A21201; RRID:AB_141630
Alexa488-donkey anti-rabbit IgG	Invitrogen	Cat# A21206; RRID:AB_2535792
Alexa594-donkey anti-mouse IgG	Invitrogen	Cat# A21203; RRID:AB_141633
Alexa594-doneky anti-rabbit IgG	Invitrogen	Cat# A21207; RRID:AB_141637
Goat anti-mouse IgG, alkaline phosphatase conjugated	thermo Fisher Scientific	Cat# A21060; RRID:AB_2536528
Goat anti-rabbbit IgG, alkaline phosphatase conjugated	thermo Fisher Scientific	Cat# A16099; RRID: AB_2534773
Histofine Simple Stain MAX PO (R)	Nichirei Bioscience	Cat# 414141F
Histofine Simple Stain MAX PO (M)	Nichirei Bioscience	Cat# 414131F

Viral strain	Sources	Identifier
SARS-CoV-2, WA-1 strain - BEI	CDC	Cat #NR-52281
SARS-CoV-2 GFP	provided by Dr. Ralph S. Baric	Hou et al.
CMV Promoter Thomson Factors Lentivirus Set	ABMgood, Canada	Cat# G353

Reagent or Resources	Sources	Identifier
Normal Donkey Serum	Sigma	Cat# D9663
PBS, pH7.4	Quality Biological	Cat# 119-069-131
Triton X100	Sigma	Cat# X100
Hydrogen peroxide (H2O2)	Sigma	Cat# H1009
Antigen Retriever, Citrate buffer, pH6	Sigma	Cat# C9999
Antigen Retriever, formic acid	Sigma	Cat# F0507
VECTASTAIN Elite Kits	VectorLab	Cat# PK-6100
SignalStain® Vibrant Red AP Substrate Kit	Cell Signal Tech	Cat# 76713
DAB (3,3′-Diaminobenzidine tetrahydrochloride hydrate)	Sigma	Cat# D5637
Hematoxylin Solution, Harris Modified	Sigma	Cat# HHS32
Tissue-Plus OCT Compound	Fisher Scientific	Cat# 23-730-571
Ammonium Nickel (II) sulfate hexahydrate	Sigma	Cat# A1827
Lithium Carbonate	Sigma	Cat# 255823
Ethanol, Decon Labs, 200 proof	VWR	Cat# 71002-426
Xylenes Histological Grade	Sigma	Cat# 534056
Thioflavin-T	Sigma	Cat# T3516
DAPI (4',6-diamidino-2-phenylindole)	Thermo Fisher Scientific	Cat# D9542
Permount mounting medium	Fisher	Cat# SP15100
Fluorescence mounting medium	Sigma	Cat# F4680
Paraformaldehyde (4%, pH7.4) in PBS	Thermo Fisher Scientific	Cat# J61889
RNAscope® 2.5 HD Reagent Kit-RED	ACD	Cat# 322350
RNAscope® Probe	ACD	Cat# 854841
Knockout DMEM medium	Thermo Fisher Scientific	Cat# 10829018
Knockout serum replacer	Thermo Fisher Scientific	Cat# 10828028
Nonessential amino acids	Thermo Fisher Scientific	Cat# 11140050
GlutaMAX	Thermo Fisher Scientific	Cat# 35050061
β-mercaptoethanol	Sigma	Cat# M3148
Recombinant human basic fibroblast growth factor	Thermo Fisher Scientific	Cat# 13256-029
Collagenase IV	Stem Cell Technologies	Cat# 17104019
DMEM/F12	Thermo Fisher Scientific	Cat# 11320033
N2 supplement	Thermo Fisher Scientific	Cat# 17502048
Neurobasal medium	Thermo Fisher Scientific	Cat# 21103049

B27 supplement	Thermo Fisher Scientific	Cat 17504044
Penicillin/streptomycin	Thermo Fisher Scientific	Cat# 15140122
Stemolecule SB431542, TGF-β inhibitor	Reprocell	Cat# 04-0010-10
LDN-193189, inhibitor of bone morphogenetic protein receptor	Reprocell	Cat# 04-0074
Matrigel	BD Biosciences	Cat# 354277
bFGF	Pepro Tech	Cat# 100-18b
EGF, epidermal growth factor	Pepro Tech	Cat# 100-47
Heparin	Sigma	Cat# H4784
Brain-derived neurotrophic factor, BDNF	Pepro Tech	Cat# 450-02
Glial cell–derived neurotrophic factor, GDNF	Pepro Tech	Cat# 450-10
X-tremeGENE siRNA transfection reagent, Roche	Sigma	Cat# 6366236001
SuperScript™ III Reverse Transcriptase kit	Thermo Fisher Scientific	Cat# 18080051
PowerUp™ SYBR™ Green Master Mix	Thermo Fisher Scientific	Cat# A25742

Brain Tissue	Source	Identifier
Alzheimer's Disease (AD)-Covid19 brain tissue, Male,	NIH NeuroBioBank	UMBN #6435
Autism-Covid19 brain tissue, Female, 38 yr	NIH NeuroBioBank	UMBN #6436
Autism-Covid19 brain tissue, Male, 30 yr	NIH NeuroBioBank	UMBN #6437
Frontotemporal Dementia (FTD)-Covid19, Female, 71 yr	UCSD,	#5922
Covid19, Male, 77 yr	UCSD,	#5932
Sporadic AD, Female, 65 yr	NIH NeuroBioBank	#116311
Sporadic AD, Male, 63 yr	NIH NeuroBioBank	#116319
Sporadic AD, Male, 63 yr	NIH NeuroBioBank	#116317
Sporadic AD, Male, 79 yr	UCSD,	#5877
Sporadic AD, Female, 71 yr	UCSD,	#5875
Sporadic AD, Male, 76 yr	UCSD,	#5872
Unaffected Control, Male, 29 yr	NIH NeuroBioBank	UMBN #1502
Unaffected Control, Male, 30 yr	NIH NeuroBioBank	UMBN #6099
Unaffected Control, Female, 38 yr	NIH NeuroBioBank	UMBN #1648
Unaffected Control, Male, 38 yr	NIH NeuroBioBank	UMBN #5249
Unaffected Control, Male, 38 yr	NIH NeuroBioBank	UMBN #4592
Unaffected Control, Female, 77 yr	NIH NeuroBioBank	UMBN #1569
Unaffected Control, Male, 75 yr	NIH NeuroBioBank	UMBN #5830
Unaffected Control, female, 76 yr	NIH NeuroBioBank	UMBN #5219
ASD-Autism, 37 yr	NIH NeuroBioBank	UMBN #5027
ASD-Autism suspended, Epilepsy, 28 yr	NIH NeuroBioBank	UMBN #5934
ASD-Autism, Epilepsy, 29 yr	NIH NeuroBioBank	UMBN #5940
ASD-Austim suspended, 35 yr	NIH NeuroBioBank	UMBN #6092
ASD-Autism suspended, 36 yr	NIH NeuroBioBank	UMBN #6212
ASD-Autism suspended, 30 yr	NIH NeuroBioBank	UMBN #6381
Frontotemporal dementia, 70yr	NIH NeuroBioBank	UMBN #6220
Frontotemporal dementia, 65yr	NIH NeuroBioBank	UMBN #6019
Frontotemporal dementia, 76yr	NIH NeuroBioBank	UMBN #6264
Frontotemporal dementia, 73yr	NIH NeuroBioBank	UMBN #6207

Cell lines	Source	Identifier
iPSCs, from Familial AD, female, 31 yr	Coriell Institute	Cat# AG25367
iPSCs, from Sporadic AD, male, 60 yr	Coriell Institute	Cat# AG07376
iPSCs, from Sporadic AD, male, 83 yr	Coriell Institute	Cat# GM24666
iPSCs, from apparently healthy male, 55 yr	Coriell Institute	Cat# GM23248
iPSCs, from apparently healthy female, 36 yr	Coriell Institute	Cat# GM23279
iPSCs, from apparently healthy female, 36 yr	Coriell Institute	Cat# GM23280
Primary human neuron	Neuromics	HNC001
Vero E6 cells	ATCC	CRL-1586
mouse embryonic fibroblasts (MEF)	Thermo Fisher Scientific	Cat# A34180

Plasmid DNAs	**Source**	**Identifier**
CRYAA2_pcDNA3.1+/C-(K)-DYK	Genscript	Cat# OHu53183D
GJA8_pcDNA3.1+/C-(K)-DYK	Genscript	Cat# OHu22749D
OTOR(NM_020157.4) ORF Clone	Genscript	Cat# OHu00520D
Human LILRB5(NM_001081442.2) ORF Clone	Genscript	Cat# OHu64562D
FCGR3A(NM_000569.6) ORF Clone	Genscript	Cat# OHu27381D
PSG6(NM_001031850.4) ORF Clone	Genscript	Cat# OHu56074D

siRNAs	**Source**	**Identifier**
GJA8 siRNA	Ambion	Cat# S5769
CRYAA2 siRNA	Ambion	Cat# 3540
PSG6 siRNA	Ambion	Cat# 11312

Lentiviru	**Source**	**Identifier**
Otoraplin (OTOR) (NM_020157) Human Tagged ORF Clone	Origene	Cat# RC210984L4V
LILRB5 (NM_001081443) Human Tagged ORF	Origene	Cat# RC219303L4V
CD16 (FCGR3A) (NM_000569) Human Tagged ORF	Origene	Cat# RC206429L2V

Software and Algorithems	Source	Identifier
GraphPad Prism 7	GraphPad	NA
photoshop CS3	Adobe	NA

QPCR primers	Sources	Identifier
FCGR3A qPCR, mRNA forward: 5'-CCTCCTGTCTAGTCGGTTTGG; reverse: 5'-TCGAGCACCCTGTACCATTGA	Genbank Accession NM_000569	PrimerBank ID 24429586a1
LILRA3 qPCR, mRNA forward: 5'-AGGAGTGGGGACGTGACTT; reverse: 5'-GGTCTGGCACGGATCTGTC	Genbank Accession NM_006865	PrimerBank ID 289547630c1
TLR8 qPCR, mRNA forward: 5'-AACTGCCAAGCTCCCTACG; reverse: 5'-CAAGGCACGCATGGAAATGG	Genbank Accession NM_138636	PrimerBank ID 257196253c3
LILRB5 qPCR, mRNA forward: 5'-GACTGATCCCTGACATACCCG; reverse: 5'-GTGTCTATCTGATGCCATGACTG	Genbank Accession NM_006840	PrimerBank ID 125987589c2
OTOR qPCR, mRNA forward: 5'-TCTGGCTAGTGCTCAAGAAGA; reverse: 5'-TAACCCACGACTCCCATCTCG	Genbank Accession NM_020157	PrimerBank ID 21618345c1
TMEM140 qPCR, mRNA forward: 5'-TCGGCTTCTATAACTTCTGCCT; reverse: 5'-CTGTTGCACTGGGCTAGGAG	Genbank Accession NM_018295	PrimerBank ID 256355110c2
SIGLEC1 qPCR, mRNA forward: 5'-ATGGGGTACGCCTCCAAAC; reverse: 5'-GTGCCTCATTGGGTGTGTTG	Genbank Accession NM_023068	PrimerBank ID 89142743c1
CCL4 qPCR, mRNA forward: 5'-CTGTGCTGATCCCAGTGAATC; reverse: 5'-TCAGTTCAGTTCCAGGTCATACA	Genbank Accession NM_002984	PrimerBank ID 4506845a1
SLCO2B1 qPCR, mRNA forward: 5'-TATGTGGACATTAACCAGATGCC; reverse: 5'-CTGTGACTGCTAAGACCTTTCG	Genbank Accession NM_001145211	PrimerBank ID 312176373c2
TM4SF4 qPCR, mRNA forward: 5'-CTGTGGTTGGATTCTTGGGAG; reverse: 5'-GGGTAGCCCCATGTACTATTGG	Genbank Accession NM_004617	PrimerBank ID 325974483c2
XAF1 qPCR, mRNA forward: 5'-GCTCCACGAGTCCTACTGTG; reverse: 5'-GTTCACTGCGACAGACATCTC	Genbank Accession NM_017523	PrimerBank ID 378925606c1
KCNQ5 qPCR, mRNA forward: 5'-TGTTGTCGATATAGAGGATGGCA; reverse: 5'-GAGTGCAGACGTGGCAAAAAT	Genbank Accession NM_001160134	PrimerBank ID 236462241c3
ANGPTL1 qPCR, mRNA forward: 5'-AGAAAGGAAAGCCGTAACATGAA; reverse: 5'-TCCCTGTATCTTGTTGCCATCT	Genbank Accession NM_004673	PrimerBank ID 38327520c3
COL21A1 qPCR, mRNA forward: 5'-GGCCACAAATAGCAGTTACCT; reverse: 5'-AGCCTTCATCAAACAACGTCTTA	Genbank Accession NM_030820	PrimerBank ID 90577174c2
KLHDC7B qPCR, mRNA forward: 5'-GCACCATGCACAACTACCTGT; reverse: 5'-ATTCGCCACCGATGGCATAG	Genbank Accession NM_138433	PrimerBank ID 206597555c1
HAND2 qPCR, mRNA forward: 5'-CGCCGACACCAAACTCTCC; reverse: 5'-TCGCCATTCTGGTCGTCCT	Genbank Accession NM_021973	PrimerBank ID 88999597c2
COMP qPCR, mRNA forward: 5'-CGAGTCCGCTGTATCAACACC; reverse: 5'-TCCGTGCAAACCTGCTTGT	Genbank Accession NM_000095	PrimerBank ID 40217842c2
SLC22A4 qPCR, mRNA forward: 5'-TGGTAGCCTTCATACTAGGAACA; reverse: 5'-TGGCAGCAGCATATAGCCAAC	Genbank Accession NM_003059	PrimerBank ID 24497489c1
PTPRH qPCR, mRNA forward: 5'-TCGCCCTATGCTGGGAAGT; reverse: 5'-TCTGCCCATACAGAGAATGTGT	Genbank Accession NM_002842	PrimerBank ID 241896923c2
FGF10 qPCR, mRNA forward: 5'-CATGTGCGGAGCTACAATCAC; reverse: 5'-CAGGATGCTGTACGGGCAG	Genbank Accession NM_004465	PrimerBank ID 4758359c1
VIT qPCR, mRNA forward: 5'-TGTGCTTGATAATTCAGGAGGGA; reverse: 5'-GATTGGACACCGTTGGAATAACT	Genbank Accession NM_001177970	PrimerBank ID 295789106c2
GJA8 qPCR, mRNA forward: 5'-GACCCTGCTGAGGACCTACAT; reverse: 5'-CCCAACTCCATCACGTTGAG	Genbank Accession NM_005267	PrimerBank ID 281182631c2

PSG6 qPCR, mRNA forward: 5'-AAGCTGCCCATGCCTTACATC; reverse: 5'-AGGTGTAGTTCCGACTCTTAGG	Genbank Accession NM_001031850	PrimerBank ID 141802170c1
Amyloid precursor protein (APP), mRNA, forward: 5'-GTCTCTCTCCCTGCTCTACAA; reverse: 5'-GGCCAAGACGTCATCTGAATAG	Genbank Accession NM_000484	Cairns et al., 2020
ABeta secretase 1 (BACE1), mRNA, forward: 5'-CCATCCTTCCGCAGCAATA; reverse: 5'-CGTAGAAGCCCTCCATGATAAC	Genbank Accession NM_012104	Cairns et al., 2020
Tumor necrosis factor alpha (TNFα), mRNA, forward: 5'-GAGGCCAAGCCCTGGTATG; reverse: 5'-CGGGCCGATTGATCTCAGC	Genbank Accession NM_000594.4	Cairns et al., 2021
Presenilin 1 (PSEN1), mRNA, forward: 5'-TGGCTACCATTAAGTCAGTCAGC; reverse: 5'-CCCACAGTCTCGGTATCTTCT	Genbank Accession NM_000021	Cairns et al., 2024
Presenilin 2 (PSEN2), mRNA, forward: 5'-CTGACCGCTATGTCTGTAGTGG; reverse: 5'-CTTCGCTCCGTATTTGAGGGT	Genbank Accession NM_012486	Cairns et al., 2025
Interleukin 6 (IL-6), mRNA, forward: 5'-TCAATATTAGAGTCTCAACCCCC; reverse: 5'-TTGTTTTCTGCCAGTGCCTC	Genbank Accession NM_012486	Cairns et al., 2026
Interleukin 1beta (IL-1β), mRNA, forward: 5'-CAGAAGTACCTGAGCTCGCC; reverse: 5'-AGATTCGTAGCTGGATGCCG	Genbank Accession NM_000576.2	Cairns et al., 2027
Interferon gamma (INFγ), mRNA, forward: 5'-ACTGTCGCCAGCAGCTAAAA; reverse: 5'-TATTGCAGGCAGGACAACCA	Genbank Accession NM_000619	Cairns et al., 2028
Glyceraldehyde 3-phosphate dehydrogenase (GAPDH), mRNA, forward: 5'-ATTGCCCTCAACGACCACT; reverse: 5'-ATGAGGTCCACCACCCTGT	Genbank Accession NM_002046.5	Cairns et al., 2030
CDC 2019-nCoV_N1, forward: 5'-GAC CCC AAA ATC AGC GAA AT	CDC	IDT, Cat# 10006821
CDC 2019-nCoV_N1, reverse: 5'-TCT GGT TAC TGC CAG TTG AAT CTG	CDC	IDT, Cat# 10006822
2019-nCoV_N_Positive Control	IDT	IDT, Cat# 10006625